

## 8. ABYSSAL PERIDOTITES FROM ODP HOLE 670A (21°10'N, 45°02'W): RESIDUES OF MANTLE MELTING EXPOSED BY NON-CONSTRUCTIVE AXIAL DIVERGENCE<sup>1</sup>

Stephen C. Komor,<sup>2</sup> Timothy L. Grove,<sup>3</sup> and Rejean Hébert<sup>4</sup>

### ABSTRACT

The Ocean Drilling Program's Hole 670A is located ~45 km south of the Kane Fracture Zone. Non-constructive (amagmatic) axial divergence ~10 km east of Hole 670A exposes residual mantle peridotites at the seafloor. The average peridotite in the group of 18 studied has 68% of its original mineralogy replaced by serpentine and related minerals. Average reconstructed (preserpentinization) modal proportions are 81.6% OL, 14.7% OPX, 2.4% CPX, and 1.3% SPINEL. Average chemical parameters are OL Mg# = 90.5, OL NiO = 0.31 wt%, OPX Mg# = 90.5, OPX Al<sub>2</sub>O<sub>3</sub> = 4.21 wt%, CPX Mg# = 90.9, CPX Na<sub>2</sub>O = 0.19 wt%, and spinel Cr# = 24.7. Chemical and mineralogical compositions of most samples fall in a restricted range, suggesting the rocks record a similarly narrow range of melting percentages. Major and trace element modeling indicate 14%–16% melting of a partially depleted source like the Tinaquillo lherzolite can account for most of the sample compositions. One harzburgite collected 30 m away from the other samples contains minerals with more refractory compositions; calculated melting percentages for this harzburgite are 18%–20%. The difference in calculated melting percentages between the refractory harzburgite and the rest of the samples may indicate that the percent of melting (or the efficiency of melt extraction) in the sub-oceanic upper mantle melting varies on a scale of tens of meters. Comparison of the Hole 670A peridotite compositions with peridotites from the KFZ reveals no significant differences. Therefore, there is no support in this small sample set for a variation of residual peridotite compositions correlative with the transform fault effect documented from basalt compositional variations.

### INTRODUCTION

The earth's upper mantle rises and partially melts beneath mid-ocean ridges. Basalt produced by partial melting is abundantly exposed at oceanic spreading centers. At most locations along spreading ridges, however, the complementary residue of melting is concealed by basalt and underlying plutonic cumulates. Most samples of abyssal residual peridotites are collected by dredging fracture zones, where in some cases the oceanic crustal section is thin, and shallow levels of the uppermost mantle are exposed at the seafloor (e.g., Stroup and Fox, 1981). However, abyssal peridotites from fracture zones may not be entirely representative of residual mantle beneath spreading ridges. Systematic correlations between basalt chemistry and proximity to fracture zones have been attributed to lower extents of mantle melting near fracture zones (Bender et al., 1984; Langmuir and Bender, 1984). If this hypothesis is correct, one might expect to find a complementary variation in the geochemistry and petrology of residual mantle peridotites with distances from fracture zones, reflecting variations in melting percentages. This report discusses the petrology of abyssal peridotites recovered by drilling at ODP Hole 670A along the Mid-Atlantic Ridge, and concludes with a comparison of the Hole 670A samples to peridotites recovered from the Kane Fracture Zone (KFZ). Comparison of the Hole 670A samples with peridotites from the KFZ provides an independent check on the proposal that systematic variations exist in the extent of melting beneath ridge segments and associated transform faults.

### GEOLOGY IN THE VICINITY OF HOLE 670A

Hole 670A on Leg 109 of the Ocean Drilling Program was spudded into sediment at 21°10'N, 45°02'W (water depth = 3615 m). The drillsite is located ~45 km south of the KFZ, and 10 km west of the axis of divergence of the Mid-Atlantic Ridge (Fig. 1). Serpentinized peridotite was penetrated beneath 6.5 m of sediment and rubble, and drilling continued in peridotite to the total depth of 92.5 m. At the ridge segment north of Hole 670A, extrusive volcanism is common, and new oceanic crust is being created by seafloor spreading (Karson et al., 1987). The spreading rate is asymmetric along this northern ridge segment; 1.7 cm/yr to the west and 1.1 cm/yr to the east (Purdy et al., 1978). The ridge segment to the south of Hole 670A shows signs of recent volcanism, but now is apparently quiescent. Hole 670A is located in a ~10-km-wide zone where no new oceanic crust is being created, but seafloor spreading continues in order to accommodate the constructional spreading ridges on either side. Karson et al. (1987) have termed this zone a zero-offset transform (Fig. 1) and describe geologic features that indicate stretching rather than constructional volcanism is occurring in the zone. The geologic setting of Hole 670A between two active or recently active magma cells may approach more closely than fracture zones the thermal and tectonic environment of normal spreading ridges. If so, peridotites recovered at Hole 670A are more representative of typical North Atlantic suboceanic mantle than the more commonly recovered fracture zone peridotites (Dick et al., 1984; Michael and Bonatti, 1985).

### ANALYTICAL METHODS

Modal proportions and grain sizes of olivine, clinopyroxene, orthopyroxene and spinel are listed in Tables 1 and 2, respectively. Grain sizes were measured using a micrometer ocular and represent the long dimensions of the measured grains. Modal data are based on 1000 points per thin section, counted on a grid spacing of 0.5 mm. Counting statistics indicate the accuracy of the measurements is approximately 1%–3% relative (Van der Plas and Tobi, 1965). How-

<sup>1</sup> Detrick, R., Honnorez, J., Bryan, W. B., Juteau, T., et al., 1990. *Proc. ODP, Sci. Results*, 106/109: College Station, TX (Ocean Drilling Program).

<sup>2</sup> U.S. Geological Survey, 821 E. Interstate Ave., Bismarck, ND 58501.

<sup>3</sup> Department of Earth, Atmospheric and Planetary Sciences 54-1220, Massachusetts Institute of Technology, Cambridge, MA 02139.

<sup>4</sup> Département de Géologie, Pavillon Pouliot, Université Laval, Sté-Foy, Quebec, Canada G1K 7P4.

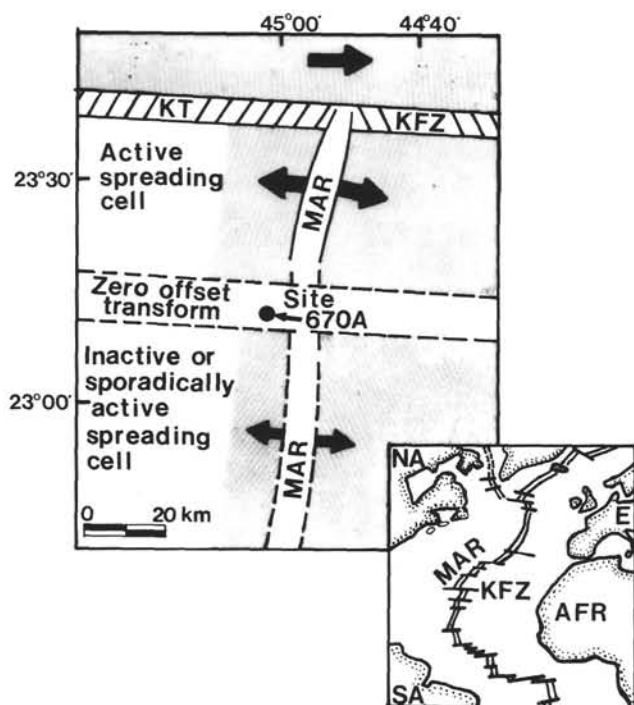


Figure 1. Generalized map showing the major tectonic elements along the Mid-Atlantic Ridge (MAR) near Hole 670A. The main features are the Kane Fracture Zone (KFZ), the Kane Transform (KT), the active spreading cell to the north of Hole 670A, the zero offset transform where Hole 670A was drilled, and the recently active spreading cell to the south. In inset: AFR, Africa; E, Europe; NA, North America; SA, South America. After Figures 1 and 4 of Karson et al. (1987).

ever, the actual accuracy must be somewhat poorer because most pyroxene grains are larger than the grid spacing.

Serpentine separates were generated by centrifuging whole rock powders in tetrabromoform ( $D = 2.98 \text{ g/cm}^3$ ). The separated light fraction was washed with distilled water and centrifuged again to ensure that all heavy minerals were removed. This procedure separates serpentine ( $D = 2.5 - 2.6 \text{ g/cm}^3$ ), talc, and chlorite ( $D = 2.6 - 2.8 \text{ g/cm}^3$ ) from olivine, pyroxenes, spinel, and magnetite, which all have densities  $\geq 3.3 \text{ g/cm}^3$  (Phillips and Griffen, 1981). The mineralogy of serpentine separates sedimented on glass slides was identified using a SCINTAG PAD 5 automated X-ray diffraction spectrometer at the University of Wisconsin (copper  $K\alpha$  radiation, voltage = 45 kV, current = 40 mA). Oxygen isotopes in serpentine separates were measured at the University of Wisconsin. Samples were reacted with  $\text{BrF}_5$ , and the liberated oxygen was converted to  $\text{CO}_2$  (Clayton and Mayeda, 1963). Isotopic ratios were measured on a Finnigan/Mat-251 triple collecting mass spectrometer. The oxygen isotope values are quoted relative to SMOW (Craig, 1961) using the standard notation (Table 3). Eighteen replicate analyses of quartz standard NBS-28 performed in the Wisconsin laboratory by SCK over a period of several months yielded an average  $\delta^{18}\text{O}$  of 9.47 per mil ( $\sigma = 0.18$  per mil).

Mineral chemistry of olivine, pyroxenes, and spinel was determined using the JEOL 733 Superprobe in the Department of Earth, Atmospheric and Planetary Sciences at the Massachusetts Institute of Technology. Operating conditions were: accelerating voltage = 15 kV, beam current = 25 nA, and, for most analyses, beam diameter = 10  $\mu\text{m}$ . Pyroxenes are exsolved on several scales in the Hole 670A samples. Some exceptionally coarse lamellae and blebs are several hundred micrometers across, although most are  $\sim 10\text{--}50 \mu\text{m}$  across. In addition, submicrometer-scale exsolution features are distributed throughout the host pyroxenes. Wherever possible, a 10- $\mu\text{m}$  beam diameter was used to obtain an average composition of host pyroxene and pyroxene exsolved on a submicrometer scale within the analysis volume. On some smaller exsolution lamellae and blebs, the spot size was reduced to 2  $\mu\text{m}$  to avoid overlap with adjacent host pyroxene.

The automated microprobe was controlled by the computer program MINQUANT (Lange and Recca, 1987; Recca et al., 1987). The methods of Bence and Albee (1968) and Albee and Ray (1970) were used to correct for matrix effects. The analyses presented in Table 4 are averages of between 5 and 16 analyses (usually 9) per phase per sample. Counting statistics indicate that accuracy and precision for major elements are better than 1% of the amount present. NiO concentrations in spinel and olivine were measured with a precision of 2%–3% by accumulating x-ray counts for 120 s on the Ni peak. Core to rim traverses were conducted to check for compositional zoning, but none was detected in any of the primary phases.

## SAMPLE SET AND PETROGRAPHY

This report presents results for 18 serpentinized peridotites recovered from sub-seafloor depths of 17–83.9 m. Reconstructions of original modal proportions suggest that prior to serpentinization the peridotites were dunites, harzburgites, and CPX-poor lherzolites.

Olivine in the samples occurs as angular fragments surrounded by mesh-textured serpentine. Original olivine grain sizes, estimated from groups of fragments with similar interference colors that extinguish simultaneously, are mostly in the range 0.5–1.3 mm. Subgrain boundaries occur within some olivine fragments.

Orthopyroxene forms large porphyroclasts up to 9.1 mm long. These are often sheared or bent, and may be stretched into elongate ovoid or ribbon-like grains that define a lineation in the peridotites. Undulatory extinction is common. Exsolved clinopyroxene is present in all orthopyroxene, both as exsolution lamellae and as granules around the orthopyroxene margins (Figs. 2A, -B). Orthopyroxenes are partially to completely replaced by bastite and may be surrounded by halos of talc. Complete pseudomorphs of orthopyroxene sometimes contain patches or veins of chlorite.

Clinopyroxene porphyroclasts may be subrounded with ragged margins or sheared, bent, and stretched into ribbon-like grains; both types commonly show undulatory extinction. Grain sizes are mostly between 0.4 and 3.1 mm. Small (<0.2 mm), equant, undeformed neoblasts of clinopyroxene are present around the margins of some orthopyroxene and clinopyroxene porphyroclasts (see Fig. 5 of Boudier, 1979). Exsolved orthopyroxene lamellae and granules are present in all clinopyroxene (Figs. 2C, -D). Thin fringes of tremolite, talc, and serpentine are observed around some clinopyroxenes. Most clinopyroxene is well-preserved in the peridotites, and it is the least altered of the three primary silicate phases.

Spinel exhibits a wide range of morphologies including small vermicular grains (0.1–0.2 mm), irregular grains with cusped margins, and elongate grains with angular to ovoid outlines. Grain sizes of the last three morphologies are 0.3–1.8 mm. Elongate spinels define a lineation subparallel to that defined by stretched pyroxenes. The margins of some spinels are altered to magnetite.

## Serpentinization

Between 49 and 92 modal% of the primary phases in Hole 670A peridotites is replaced by serpentine and minor amounts of related minerals, including magnetite, chlorite, and talc (Table 1). The average extent of replacement of primary minerals is fairly constant at  $68\% \pm 10\%$  ( $\pm 1 \sigma$ ). Most serpentine occurs in a homogeneous mesh texture replacing olivine. Vein serpentine is also observed, but is volumetrically much less abundant than the massive mesh texture type. Powder x-ray diffraction analyses of serpentine separates show that they are composed mostly of 1T-lizardite (PDF No. 18-779); also detected in smaller abundances were aluminian 1T-lizardite (PDF No. 11-386), 2M clinochrysoile (PDF No.

**Table 1. Measured modes (reconstructed primary modes).**

Sample	(m)	OL	OPX	CPX	SPIN	SERP	MAGN	OTHER	PRIMARY RK TYPE	
109 670A 2M-01	20-23	17	10 (81)	14 (18)	- -	1 (1)	64	11	-	H
109 670A 5R-01	8-11	45.3	27 (82)	10 (14)	3 (3)	1 (1)	57	2	-	H
109 670A 5R-02	78-80	46	34 (90)	- (9)	- -	1 (1)	60	2	3% CHLR	D
109 670A 5R-02	87-89	46.1	8 (99)	-	- -	- (1)	91	1	-	D
109 670A 5R-02	118-120	46.4	23 (81)	1 (16)	- (2)	tr (1)	70	5	1% CHLR	H
109 670A 5R-02	139-142	46.6	24 (79)	12 (19)	tr (1)	tr (1)	62	2	-	H
109 670A 6R-01	4-6	54.6	25 (79)	14 (16)	3 (4)	- (1)	58	tr	-	H
109 670A 6R-01	19-22	54.8	19 (80)	15 (15)	2 (4)	tr (1)	55	1	8% BST	H
109 670A 6R-01	25-27	54.9	26 (80)	11 (14)	5 (5)	tr (1)	57	tr	1% CHLR	L
109 670A 6R-01	38-40	55	23 (81)	5 (15)	2 (3)	1 (1)	62	2	5% BST	H
109 670A 6R-01	54-56	55.1	27 (78)	7 (17)	2 (4)	1 (1)	56	2	5% BST	H
109 670A 7R-01	2-4	64	22 (92)	tr (6)	- -	1 (2)	73	4	-	D
109 670A 7R-01	25-27	64.3	16 (78)	15 (19)	1 (2)	tr (1)	66	2	-	H
109 670A 8R-01	6-8	73.6	26 (73)	20 (21)	4 (5)	1 (1)	44	5	-	L
109 670A 8R-01	12-14	73.6	14 (79)	11 (14)	5 (6)	tr (1)	69	1	-	L
109 670A 8R-01	32-36	73.8	17 (78)	16 (19)	1 (2)	tr (2)	65	1	-	H
109 670A 9R-01	63-65	83.6	23 (85)	4 (15)	- -	tr (0.5)	67	6	-	H
109 670A 9R-01	94-97	83.9	6 (74)	12 (18)	6 (7)	1 (1)	70	5	-	L

<sup>1</sup> Measured modes based on 1000 points per thin section (1315 points for 670A-9R-1, 94-97 cm). Grid spacing = 0.5 mm.

<sup>2</sup> Reconstructed modes based on pseudomorph identification and assuming constant volume serpentinization.

<sup>3</sup> Depth measured from seafloor.

<sup>4</sup> OL, olivine; OPX, orthopyroxene; CPX, clinopyroxene; SPIN, spinel; SERP, serpentine—category includes lizardite, chrysotile, and antigorite; MAGN, magnetite; CHLR, chlorite; BST, bastite.

<sup>5</sup> 670A-6R-1, 19-22 cm, includes a trace of tremolite.

<sup>6</sup> D, dunite; H, harzburgite; L, lherzolite.

31-808), and orthochrysotile (PDF No. 25-645). The criteria of Whittaker and Zussman (1956) were used to identify the serpentine phases. Although small amounts of antigorite, talc, and chlorite are observed in some thin sections, reflections for these phases were not identified in the x-ray diffraction analyses. The absence of these phases from the x-ray diffractograms is probably due to their low modal abundances.

Oxygen isotopic values of serpentine separates are  $\delta^{18}\text{O} = 3.7\text{--}8.8$  per mil (Table 3). Temperatures of serpentinization can be estimated using Wenner and Taylor's (1971) empirical serpentine-water thermometer, as recalculated by Harper et al. (1988, their Table 6). Application of this geothermometer to the isotopic data results in calculated serpentinization temperatures of  $113\text{--}246^\circ\text{C}$  (average =  $170^\circ\text{C}$ ), assuming the serpentinizing fluid was seawater with  $\delta^{18}\text{O} = 0$  per mil, or  $160\text{--}385^\circ\text{C}$  (average =  $251^\circ\text{C}$ ) if the serpentinizing fluid was

Mid Atlantic Ridge hydrothermal water with  $\delta^{18}\text{O} = +2.4$  per mil (Campbell et al., 1988). Phase equilibria in the serpentine mineral system (Evans et al., 1976) indicate that at crustal pressures, chrysotile and antigorite coexist between  $200^\circ$  and  $300^\circ\text{C}$ , but below  $200^\circ\text{C}$ , antigorite reacts to chrysotile + talc. The mineral assemblage observed in most of the serpentinites (i.e., chrysotile + lizardite  $\pm$  antigorite  $\pm$  talc), and the average temperatures calculated from isotopic data ( $170^\circ$  and  $251^\circ\text{C}$ ), suggest that serpentinization occurred at P-T conditions similar to those of the antigorite-out reaction boundary (also see Bonatti et al., 1984).

### Modal Reconstructions

Reconstructed primary modes (Table 1, Fig. 3) are estimated by assigning mesh texture serpentine pseudomorphs and associated magnetite to the primary olivine category;

**Table 2. Grain sizes\* (mm)**

Sample	OL	OPX	CPX	SPIN	
109 670A 2M-01	20-23	0.3-2.9	0.9-4.4;9.1	—	ND
109 670A 5R-01	8-11	0.3-1.3	0.8-3.9	0.4-0.7	0.1-1.2
109 670A 5R-02	78-800	0.3-1.3	—	—	ND
109 670A 5R-02	87-890	0.3-1.3	—	—	1.2
109 670A 5R-02	118-120	0.4-0.8	1.8-3.3	—	1.5-1.8
109 670A 5R-02	139-142	0.4-1.0	1.5-5.1	0.2-0.3	0.1-0.5
109 670A 6R-01	4-6	0.8-1.0	0.7-5.2	1.2-3.1	1.5
109 670A 6R-01	19-22	0.5-1.3	1.0-8.0	0.8-1.3	0.1-0.6
109 670A 6R-01	25-27	1.0-1.3	0.5-3.9	0.7-4.4	ND
109 670A 6R-01	38-40	0.5-1.0	1.6-4.4;9.1	0.4-1.0	0.2-1.0
109 670A 6R-01	54-56	0.5-1.0	1.3-6.8	0.5-2.9	0.3-0.8
109 670A 7R-01	2-4	0.5-1.0	0.5	—	0.4-1.3
109 670A 7R-01	25-27	0.5-1.0	1.0;9.1	0.2-0.4	ND
109 670A 8R-01	6-8	0.8-2.3	1.8-9.6	1.3-6.2	0.1-1.8
109 670A 8R-01	12-14	1.2-1.8	1.8-9.2	2.1-3.1	0.2-0.6
109 670A 8R-01	32-36	0.8-1.8	1.3-5.7	1.0-2.1	0.8-1.8
109 670A 9R-01	63-65	0.8-2.9	1.3-3.9	1.1	0.1-0.4

ND—Not Determined

\*Estimates of pre-serpentinization dimensions based on measurements of primary grains and pseudomorphs.

Table 3. Oxygen isotopes in serpentinite separates.

Sample	Serpentine ( $\delta^{18}\text{O}$ )	Calculated temperature of fluid-rock interaction ( $^{\circ}\text{C}$ ), assuming fluid is:	
		Seawater ( $\delta^{18}\text{O} = 0$ )	<sup>1</sup> MARK hydrothermal fluid ( $\delta^{18}\text{O} = +2.4$ )
109-670A-			
2M-1 20-23	8.8	113	160
6R-1 19-22	7.3	141	202
6R-1 38-40	6.2	166	241
6R-1 54-56	4.8	208	311
7R-1 10-12	4.3	223	340
7R-1 25-27	6.8	152	218
8R-1 6-8	6.7	154	222
9R-1 10-12	3.7	246	385
9R-1 63-65	8.1	125	178
	Average	170	251
	Standard deviation	41	69

<sup>1</sup> Campbell et al. (1988).

bastite pseudomorphs and fringing talc to primary orthopyroxene; thin tremolite fringes around some clinopyroxenes to primary clinopyroxene; and magnetite rimming spinel to primary spinel. The average pre-serpentinization mode estimated for all samples is 81.6% olivine, 14.7% orthopyroxene, 2.4% clinopyroxene, and 1.3% spinel. The estimate for thirteen clinopyroxene-bearing samples is 78.6% olivine, 16.7% orthopyroxene, 3.3% clinopyroxene, and 1.4% spinel (Table 5).

If no volume changes occurred during serpentinization, these are accurate estimates of the pre-serpentinization modal proportions. However, if serpentinization was not a constant-volume process, the reconstructed modal mineralogy is in error because, in general, volume changes are unequally distributed among mineral phases in peridotites. Unequal distribution of volume changes stems from the differing susceptibilities of minerals to serpentinization. Hydrothermal experiments by Janecky and Seyfried (1986) in which lherzolite was reacted with seawater at 200 $^{\circ}\text{C}$ , show that serpentinization rates are greatest for OPX, intermediate for OL, and slowest for CPX. This is in accord with petrographic observations showing that clinopyroxene is least affected by serpentinization. Volume increases during serpentinization cause clinopyroxene abundances to be underestimated in reconstructed modes, whereas olivine and orthopyroxene are overestimated (Komor et al., 1985). Therefore, estimates of original clinopyroxene abundances made assuming no volume increase (Table 1) represent minimum estimates of pre-serpentinization clinopyroxene abundances. Furthermore, since clinopyroxene abundances decrease during partial melting of lherzolites (e.g., Mysen and Kushiro, 1977), the reconstructed modal data represent most-refractory estimates for residues of partial melting.

### MINERAL CHEMISTRY

Mineral chemistry is presented in Table 4. Olivine has a narrow range of compositions, with Mg#’s ( $100 \times \text{Mg}/(\text{Mg} + \text{Fe})$ ) = 90.1–90.9 and NiO = 0.29–0.34 wt% (Fig. 4). There is no systematic variation of olivine Mg# with depth (Fig. 4). Mg#’s of orthopyroxene porphyroclasts are in the range 90.2–91.1, and  $\text{Al}_2\text{O}_3$  contents are 3.6–4.8 wt%. The average orthopyroxene has a quadrilateral composition of  $\text{Wo}_{3.6}\text{Fs}_{9.5}\text{En}_{86.9}$ . Exsolved orthopyroxene has higher  $\text{Al}_2\text{O}_3$  and  $\text{Cr}_2\text{O}_3$  concentrations, and lower Mg#’s, and  $\text{Na}_2\text{O}$ ,  $\text{TiO}_2$ , and CaO concentrations than orthopyroxene porphyroclasts (Fig. 5). No compositional difference was detected between orthopyroxene lamellae and granules. Clinopyroxenes have Mg#’s between 90.4 and 91.5 and an average quadrilateral

composition of  $\text{Wo}_{46.1}\text{Fs}_{3.9}\text{En}_{50.0}$ . Compared to clinopyroxene porphyroclasts, clinopyroxene exsolved from orthopyroxene hosts has lower  $\text{Al}_2\text{O}_3$  and  $\text{Cr}_2\text{O}_3$  concentrations, and higher Mg#, and  $\text{Na}_2\text{O}$ ,  $\text{TiO}_2$ , and CaO concentrations (Fig. 6). Spinel Mg#’s range from 71.3 to 75.2, and Cr#’s ( $100 \times \text{Cr}/(\text{Cr} + \text{Al})$ ) from 21.4 to 37.5 (Fig. 7).  $\text{TiO}_2$  concentrations in spinel are low, averaging 0.7 wt%.

With limited exceptions, mineral compositions are extremely uniform throughout the sample set. One exception is Sample 109-670A-5R-2, 87–89 cm, an extensively serpentinized dunite that contains  $\text{Fo}_{90.1}$  olivine, a composition somewhat more iron-rich than olivine in other samples. Also exceptional is the shallowest sample, harzburgite 109-670A-2M-1, 20–23 cm, which is distinguished by higher Mg#’s in olivine and orthopyroxene, higher Cr#’s in spinel and  $\text{Cr}_2\text{O}_3$  in orthopyroxene, and lower  $\text{Al}_2\text{O}_3$  in orthopyroxene. Incongruously, this sample also has high  $\text{Na}_2\text{O}$  in orthopyroxene, and NiO in olivine no higher than in other samples. The distinct chemical characteristics of 109-670A-2M-1, 20–23 cm do not appear to be attributable to more extensive serpentinization because modal serpentinite (64%) in the sample is very similar to that of other samples (Table 1).

### GEOOTHERMOMETRY

Temperatures of equilibration for the Hole 670A peridotites can be estimated from two pyroxene thermometry (Wells, 1977; Kretz, 1982; Lindsley and Anderson, 1983; Bertrand and Mercier, 1985) and from olivine-spinel thermometry (Fabries, 1979). Wells’ (1977) calibration of Fe-Mg partitioning between orthopyroxene and clinopyroxene yields an average equilibration temperature of 1063 $^{\circ}\text{C}$  (Fig. 8). Kretz’s (1982) geothermometer calibrates the temperature-dependent transfer of the En component between low and high calcium pyroxene, and indicates an average equilibration temperature of 969 $^{\circ}\text{C}$ . Bertrand and Mercier’s (1985) calibration of the En-transfer reaction yields an average estimate of 1025 $^{\circ}\text{C}$ . Pyroxene compositions are projected from non-QUAD components onto the graphical geothermometer of Lindsley and Anderson (1983) in Figure 9. Clinopyroxene porphyroclasts, lamellae, and granules indicate temperatures of 1200–1300 $^{\circ}\text{C}$ . Orthopyroxene porphyroclasts indicate temperatures of 1100–1300 $^{\circ}\text{C}$ , with temperatures down to 800 $^{\circ}\text{C}$  inferred from exsolved orthopyroxene. Temperatures estimated from Fabries’ (1979) calibration of the olivine-spinel Mg-Fe exchange average 840 $^{\circ}\text{C}$  (Fig. 10).

The coarse exsolution observed in Hole 670A pyroxenes indicates that temperatures inferred from porphyroclasts and exsolved pyroxene reflect subsolidus rather than magmatic equilibration conditions. To estimate temperatures of magmatic equilibration, we reintegrated exsolved and host porphyroclast pyroxene for an orthopyroxene (6.8 mm) and clinopyroxene (2.5 mm) in Sample 109-670A-6R-1, 54–56 cm. This was accomplished by point counting enlarged back-scattered electron images of the pyroxenes, which clearly distinguish orthopyroxene from clinopyroxene. The scale of enlargement was such that 1 cm on the photographs = 200  $\mu\text{m}$  on the pyroxene (i.e., 50 to 1). To facilitate point counting, a fine mechanical dot pattern (7 dots/cm) was photocopied onto an overhead transparency. The transparency was overlaid on the back-scattered electron images, and the regions of ortho- and clinopyroxene outlined with a felt-tip pen. All of the coarsely exsolved pyroxene could be distinguished at the scale used for this analysis, but some of the pyroxene exsolved at a finer scale was lumped with the host. Of 22,685 points counted on a host orthopyroxene porphyroclast, 907 landed on exsolved clinopyroxene; 426 of

5455 points counted on a host clinopyroxene landed on exsolved orthopyroxene. These data indicate that the orthopyroxene host contains 4.0% exsolved clinopyroxene, and the clinopyroxene host contains 7.8% exsolved orthopyroxene. These percentages were multiplied by the compositions of exsolved and host pyroxenes to calculate reintegrated pyroxene compositions for 109-670A-6R-1, 54–56 cm. Petrographic observations show that the degree of exsolution is roughly the same in all Hole 670A pyroxenes. Therefore, average reintegrated pyroxene compositions were calculated using the percentages of exsolution estimated from 109-670A-6R-1, 54–56 cm and average host and exsolved pyroxene compositions (Table 5).

Equilibration temperatures calculated for reintegrated pyroxenes by the Wells (1977) and Bertrand and Mercier (1985) formulations are near 1170°C, and near 1120°C by Kretz's (1982) method (Fig. 8). Projected compositions of reintegrated clinopyroxene and orthopyroxene in Lindsley and Anderson's (1983) geothermometer plot near the 1300°C isotherm (Fig. 9). The Lindsley-Anderson geothermometer is known to yield high temperature estimates for aluminous pyroxenes (Anderson and Lindsley, 1984). This may explain why the Lindsley-Anderson geothermometer yields higher temperatures than the other geothermometers for the Leg 109 pyroxenes (with ~3.5–5.5 wt% Al<sub>2</sub>O<sub>3</sub>). Despite this known problem with the Lindsley-Anderson calibration, comparison with experiments suggests that 1300°C is a reasonable temperature estimate for magmatic equilibration during partial melting of peridotites beneath oceanic spreading ridges (see below). The lower temperatures indicated by the other two-pyroxene geothermometers may represent post-melting, subsolidus reequilibration of pyroxene pairs during mantle upwelling. Spinel-olivine Mg-Fe exchange equilibrium clearly was achieved at subsolidus temperatures.

#### EVIDENCE THAT THE HOLE 670A PERIDOTITES ARE RESIDUES OF PARTIAL MELTING

There are two candidate origins for the Hole 670A peridotites. They may be residues remaining after extraction of a basaltic melt from the sub-oceanic upper mantle, or cumulates crystallized from MgO-rich basalt in the lower portions of a magma chamber. Ophiolite studies show that basal ultramafic cumulates and residual upper mantle peridotites share many textural and chemical characteristics (e.g., George, 1978; Casey et al., 1981; Elthon et al., 1982). Both cumulates and restites are plastically deformed, and both are depleted in fusible elements with low rock/melt distribution coefficients. However, there are many features of the Hole 670A peridotites that are consistent with a residual origin, and no features that strongly suggest a cumulate origin; the features suggesting a residual origin are:

1. Magmatic cumulates often exhibit phase layering, defined by abrupt variations in modal proportions. In contrast, the Hole 670A peridotites are lithologically monotonous, with only small variations in pyroxene and olivine abundances and no phase layering. Restricted variations in lithology are considered by Dick (1977) to be one of the diagnostic features of residues of partial melting.

2. Cryptic mineral chemistry variation with stratigraphic height is often found in igneous cumulates. For example, the Mg# of olivine varies with stratigraphic height in cumulates in response to change in liquid composition during fractional crystallization (e.g., Irvine and Smith, 1967). As indicated in Figure 4, there is no systematic variation of olivine Mg# with depth in the Hole 670A borehole.

3. If the Hole 670A peridotites represent ultramafic cumulates, one might expect to find overlying more evolved gabbros and basalts. However, none of these more differentiated lithologies were encountered, except for minor basalt rubble at the top of the borehole.

4. In general, the Hole 670A peridotites have uniform compositions with only restricted chemical variations. Narrow compositional ranges are expected for residues of partial melting if they represent a similarly narrow range of melting percentages.

5. Compared to abyssal peridotites identified as cumulates (Hodges and Papike, 1976; Hebert et al., 1983), Hole 670A peridotites are depleted in low-distribution-coefficient elements removed by low to moderate degrees of partial melting (e.g., they contain <1 ppm Zr (L. Autio, unpubl. data)). Similarly, they are enriched in high-distribution-coefficient elements that concentrate in residues of partial melting (NiO, Cr<sub>2</sub>O<sub>3</sub>, MgO).

6. Mineral fabrics in the peridotites are indicative of high temperature ductile deformation (>1000°C; Nicolas and Violette, 1982). This type of deformation is expected in mantle peridotites that upwell and diverge beneath a spreading ridge axis.

#### ESTIMATES OF MELTING PERCENTAGES

Systematic mineralogical and chemical changes in peridotite compositions result from increasing degrees of partial melting. These include a gradual decrease and eventual elimination of modal clinopyroxene (after ~25% melting) and orthopyroxene (after ~40% melting), an increase in the Mg#'s of silicate phases, an increase in spinel Cr#, and a decrease in the Al<sub>2</sub>O<sub>3</sub> content of orthopyroxene (Dick and Fisher, 1983). The Hole 670A samples show very limited variation in these parameters, suggesting that they represent a restricted range in the extent of melting. Only one sample, clinopyroxene-free harzburgite 109-670A-2M-1, 20–23 cm, has chemical characteristics consistent with greater degrees of partial melting (Figs. 4, 5, and 7). Although the reconstructed modes for some other samples lack clinopyroxene (Table 1), their chemistries are all very similar and do not indicate appreciable differences in melting percentages.

We used three methods to estimate the percent melting, all of which assume that liquid and residue are in equilibrium until they are separated. Two of the methods involve whole rock major element compositions, and the third uses mineral trace element concentrations.

1. Whole rock major element data can be used to calculate the percent of melting if compositional data are available for the source peridotite prior to melting, the melt, and the residual peridotite. A whole rock major element composition representing the residue was calculated using average Hole 670A mineral chemistry, modal, and density data (Table 5). In order to minimize the possible influence of serpentinization on modal clinopyroxene abundances, the mode used in these calculations is the average of 13 clinopyroxene-bearing samples. Figure 11 shows the calculated average residue plotted in terms of normative olivine, clinopyroxene, and orthopyroxene. Also plotted for comparison is the average measured Hole 670A peridotite composition (L. Autio, unpubl. data). Representative source compositions plotted in the diagram are the Tinaquillo lherzolite, representing partially depleted, MORB-source mantle (Jaques and Green, 1980; Frey, 1983; Thompson, 1987), and pyrolite, representing fertile mantle (Ringwood, 1975). Melt compositions at 10 and 15 kbar are those determined by Stolper (1980) for equilibrium among liquid, olivine, clinopyroxene, and orthopyroxene. The 8-kbar phase equilibrium is from the experimental data of Takahashi and Kushiro (1983, Runs 28–33). Application of the lever rule to the residue and melt compositions allows construction of

Table 4. Mineral chemistry (wt%).

	109-670A-2M-1, 20-23 cm			SP	109-670A-5R-1, 8-11 cm			
	OL	OPX			OL	CPX	OPX	SP
SiO <sub>2</sub>	40.86	54.90	0.12	SiO <sub>2</sub>	40.58	50.63	54.16	0.03
TiO <sub>2</sub>		0.06	0.11	TiO <sub>2</sub>		0.14	0.06	0.05
Al <sub>2</sub> O <sub>3</sub>		3.59	36.93	Al <sub>2</sub> O <sub>3</sub>		5.53	4.46	47.14
Cr <sub>2</sub> O <sub>3</sub>		0.97	32.96	Cr <sub>2</sub> O <sub>3</sub>		1.18	0.77	21.34
FeO	8.84	5.60	13.49	FeO	9.38	3.10	6.05	13.14
MnO	0.12	0.13	0.17	MnO	0.13	0.12	0.15	0.15
NiO	0.30		0.16	NiO	0.30			0.22
MgO	49.76	32.22	16.84	MgO	49.15	16.79	31.65	18.30
CaO	0.08	1.87		CaO	0.07	21.41	1.98	
Na <sub>2</sub> O		0.11		Na <sub>2</sub> O		0.17	0.01	
Total	99.97	99.46	100.79	Total	99.60	99.07	99.30	100.37
Mg#	90.94	91.11	71.29	Mg#	90.33	90.61	90.31	74.30
Cr#		15.52	37.45	Cr#		12.45	10.24	23.29

	109-670A-5R-2, 78-80 cm			SP	109-670A-5R-2, 87-89 cm			
	OL				OL			
SiO <sub>2</sub>	40.87		0.04	SiO <sub>2</sub>	40.64			
TiO <sub>2</sub>			0.06	TiO <sub>2</sub>				
Al <sub>2</sub> O <sub>3</sub>			46.55	Al <sub>2</sub> O <sub>3</sub>				
Cr <sub>2</sub> O <sub>3</sub>			21.74	Cr <sub>2</sub> O <sub>3</sub>				
FeO	9.27		13.54	FeO	9.54			
MnO	0.13		0.16	MnO	0.13			
NiO	0.29		0.22	NiO	0.29			
MgO	49.37		17.98	MgO	48.87			
CaO	0.05			CaO	0.05			
Na <sub>2</sub> O				Na <sub>2</sub> O				
Total	99.98		100.29	Total	99.53			
Mg#	90.47		73.37	Mg#	90.13			
Cr#			23.85	Cr#				

	109-670A-5R-2, 118-120 cm			SP	109-670A-5R-2, 139-142 cm			
	OL	OPX			OL	CPX	OPX	SP
SiO <sub>2</sub>	40.15	53.55	0.02	SiO <sub>2</sub>	40.71	51.69	55.21	0.04
TiO <sub>2</sub>		0.06	0.06	TiO <sub>2</sub>		0.16	0.06	0.06
Al <sub>2</sub> O <sub>3</sub>		4.79	45.95	Al <sub>2</sub> O <sub>3</sub>		4.74	4.23	45.97
Cr <sub>2</sub> O <sub>3</sub>		0.91	22.29	Cr <sub>2</sub> O <sub>3</sub>		1.09	0.82	21.95
FeO	9.34	5.99	13.26	FeO	9.12	2.82	5.96	13.56
MnO	0.14	0.15	0.16	MnO	0.14	0.11	0.16	0.17
NiO	0.30		0.23	NiO	0.31			0.23
MgO	49.13	31.73	18.07	MgO	49.16	17.12	32.10	17.79
CaO	0.03	1.85		CaO	0.50	22.34	1.46	
Na <sub>2</sub> O		0.03		Na <sub>2</sub> O		0.25	0.04	
Total	99.51	99.05	100.05	Total	90.48	100.32	100.04	99.77
Mg#	90.37	90.42	73.99	Mg#	90.58	91.54	90.56	73.13
Cr#		11.21	24.56	Cr#		13.25	11.28	24.26

	109-670A-6R-1, 4-6 cm			SP	109-670A-6R-1, 19-22 cm			
	OL	CPX	OPX		OL	CPX	OPX	SP
SiO <sub>2</sub>	40.80	51.36	55.04	SiO <sub>2</sub>	40.49	50.91	54.55	0.10
TiO <sub>2</sub>		0.16	0.08	TiO <sub>2</sub>		0.10	0.05	0.05
Al <sub>2</sub> O <sub>3</sub>		5.07	4.09	Al <sub>2</sub> O <sub>3</sub>		5.40	4.75	48.73
Cr <sub>2</sub> O <sub>3</sub>		1.34	0.90	Cr <sub>2</sub> O <sub>3</sub>		1.12	0.82	19.77
FeO	9.10	3.01	5.82	FeO	9.23	3.10	5.94	12.82
MnO	0.13	0.11	0.16	MnO	0.13	0.10	0.14	0.13
NiO	0.31			NiO	0.31			0.21
MgO	49.10	17.19	31.36	MgO	49.63	17.33	31.36	18.22
CaO	0.05	21.80	2.65	CaO	0.04	21.54	2.29	
Na <sub>2</sub> O		0.27	0.07	Na <sub>2</sub> O		0.03	0.03	
Total	99.49	100.31	100.14	Total	99.81	99.72	99.92	100.03
Mg#		91.06	90.57	Mg#	90.55	90.93	90.39	73.61
Cr#		14.90	13.02	Cr#		12.12	10.19	21.39

	109-670A-6R-1, 25-27 cm				SP	109-670A-6R-1, 38-40 cm			
	OL	CPX	OPX			OL	CPX	OPX	SP
SiO <sub>2</sub>	40.61	50.49	54.90	0.06	SiO <sub>2</sub>	40.54	51.03	54.98	0.05
TiO <sub>2</sub>		0.10	0.04	0.05	TiO <sub>2</sub>		0.15	0.05	0.07
Al <sub>2</sub> O <sub>3</sub>		5.80	4.25	48.60	Al <sub>2</sub> O <sub>3</sub>		5.23	3.70	46.81
Cr <sub>2</sub> O <sub>3</sub>		1.25	0.71	20.02	Cr <sub>2</sub> O <sub>3</sub>		1.08	0.63	21.05
FeO	9.22	3.05	6.07	12.94	FeO	9.38	2.89	6.10	13.73
MnO	0.14	0.10	0.16	0.15	MnO	0.15	0.10	0.14	0.15
NiO	0.32			0.22	NiO	0.31			0.24
MgO	49.92	17.09	31.97	18.32	MgO	49.75	16.44	32.39	18.41
CaO	0.03	21.82	1.46		CaO	0.05	22.25	1.27	
Na <sub>2</sub> O		0.15	0.03		Na <sub>2</sub> O		0.17	0.01	

Table 4 (continued).

	109-670A-6R-1, 25–27 cm					109-670A-6R-1, 38–40 cm			
	OL	CPX	OPX	SP		OL	CPX	OPX	SP
Total	100.23	99.86	99.58	100.36	Total	100.18	99.33	99.28	100.51
Mg#	90.61	90.89	90.38	73.92	Mg#	90.43	91.03	90.44	74.86
Cr#		12.63	9.85	21.65	Cr#		12.06	10.06	23.18
	109-670A-6R-1, 54–56 cm					109-670A-7R-1, 2–4 cm			
	OL	CPX	OPX	SP		OL	CPX	OPX	SP
SiO <sub>2</sub>	40.60	51.10	54.66	0.08	SiO <sub>2</sub>	40.55		54.99	0.07
TiO <sub>2</sub>		0.14	0.06	0.07	TiO <sub>2</sub>			0.06	0.09
Al <sub>2</sub> O <sub>3</sub>		5.24	4.09	46.68	Al <sub>2</sub> O <sub>3</sub>			3.60	45.94
Cr <sub>2</sub> O <sub>3</sub>		1.17	0.76	21.33	Cr <sub>2</sub> O <sub>3</sub>			0.60	21.97
FeO	9.44	3.04	6.18	13.66	FeO	9.33		6.13	13.47
MnO	0.15	0.12	0.27	0.16	MnO	0.16		0.15	0.16
NiO	0.32			0.24	NiO	0.31			0.23
MgO	49.95	16.62	31.92	18.20	MgO	49.82		32.51	18.42
CaO	0.04	21.85	1.65		CaO	0.08		1.33	
Na <sub>2</sub> O		0.17	0.02		Na <sub>2</sub> O			0.01	
Total	100.50	99.46	99.61	100.42	Total	100.25		99.38	100.36
Mg#	90.41	90.69	90.21	74.10	Mg#	90.50		90.44	75.19
Cr#		13.08	11.11	23.47	Cr#			9.76	24.28
	109-670A-7R-1, 25–27 cm					109-670A-8R-1, 6–8 cm			
	OL	CPX	OPX	SP		OL	CPX	OPX	SP
SiO <sub>2</sub>	40.76	50.85	54.18	0.02	SiO <sub>2</sub>	40.16	50.72	54.41	0.05
TiO <sub>2</sub>		0.16	0.08	0.09	TiO <sub>2</sub>		0.16	0.06	0.07
Al <sub>2</sub> O <sub>3</sub>		5.40	4.50	45.32	Al <sub>2</sub> O <sub>3</sub>		5.39	4.39	46.30
Cr <sub>2</sub> O <sub>3</sub>		1.27	0.88	22.48	Cr <sub>2</sub> O <sub>3</sub>		1.20	0.83	21.37
FeO	9.28	3.17	6.11	13.77	FeO	9.18	2.96	6.05	13.58
MnO	0.14	0.12	0.15	0.16	MnO	0.14	0.12	0.15	0.17
NiO	0.32			0.24	NiO	0.33			0.25
MgO	49.26	16.70	31.60	17.86	MgO	49.27	16.36	31.78	18.39
CaO	0.06	21.24	1.65		CaO	0.06	22.15	1.88	
Na <sub>2</sub> O		0.21	0.03		Na <sub>2</sub> O		0.21	0.05	
Total	99.82	99.11	99.18	99.94	Total	99.15	99.27	99.60	100.19
Mg#	90.45	90.38	90.21	73.51	Mg#	90.54	90.78	90.35	75.12
Cr#		13.70	11.43	24.97	Cr#		13.06	11.33	23.65
	109-670A-8R-1, 12–14 cm					109-670A-8R-1, 32–36 cm			
	OL	CPX	OPX	SP		OL	CPX	OPX	SP
SiO <sub>2</sub>	40.59	50.52	54.60	0.06	SiO <sub>2</sub>	40.36	50.85	54.57	0.23
TiO <sub>2</sub>		0.14	0.06	0.07	TiO <sub>2</sub>		0.11	0.05	0.07
Al <sub>2</sub> O <sub>3</sub>		5.45	4.34	44.91	Al <sub>2</sub> O <sub>3</sub>		5.50	4.35	44.95
Cr <sub>2</sub> O <sub>3</sub>		1.31	0.83	22.15	Cr <sub>2</sub> O <sub>3</sub>		1.24	0.84	22.45
FeO	9.35	3.06	6.11	14.81	FeO	9.38	3.10	5.96	14.21
MnO	0.15	0.14	0.18	0.18	MnO	0.14	0.15	0.14	0.15
NiO	0.34			0.25	NiO	0.31			0.22
MgO	49.60	16.52	31.67	17.69	MgO	49.59	17.21	31.83	18.13
CaO	0.02	21.73	1.98		CaO	0.05	21.60	1.96	
Na <sub>2</sub> O		0.24	0.06		Na <sub>2</sub> O		0.12	0.01	
Total	100.05	99.11	99.84	100.12	Total	99.86	99.86	99.71	100.41
Mg#	90.43	90.59	90.23	73.04	Mg#	90.41	90.85	90.50	74.38
Cr#		13.87	11.44	24.86	Cr#		13.24	11.44	25.09
	109-670A-9R-1, 63–65 cm					109-670A-9R-1, 94–97 cm			
	OL	CPX	OPX	SP		OL	CPX	OPX	SP
SiO <sub>2</sub>	40.26		54.54		SiO <sub>2</sub>	40.63	51.40	55.18	
TiO <sub>2</sub>			0.04		TiO <sub>2</sub>		0.08	0.04	
Al <sub>2</sub> O <sub>3</sub>			4.45		Al <sub>2</sub> O <sub>3</sub>		4.96	3.76	
Cr <sub>2</sub> O <sub>3</sub>			0.91		Cr <sub>2</sub> O <sub>3</sub>		1.37	0.88	
FeO	9.23		5.82		FeO	9.37	3.05	5.97	
MnO	0.13		0.13		MnO	0.12	0.08	0.14	
NiO	0.33				NiO	0.32			
MgO	49.36		31.35		MgO	49.49	17.79	31.99	
CaO	0.09		2.05		CaO	0.04	21.47	2.07	
Na <sub>2</sub> O			0.00		Na <sub>2</sub> O		0.24	0.04	
Total	99.42		99.28		Total	100.44	100.44	100.06	
Mg#	90.54		90.57		Mg#	90.48	91.23	90.52	
Cr#			12.02		Cr#		15.54	13.56	

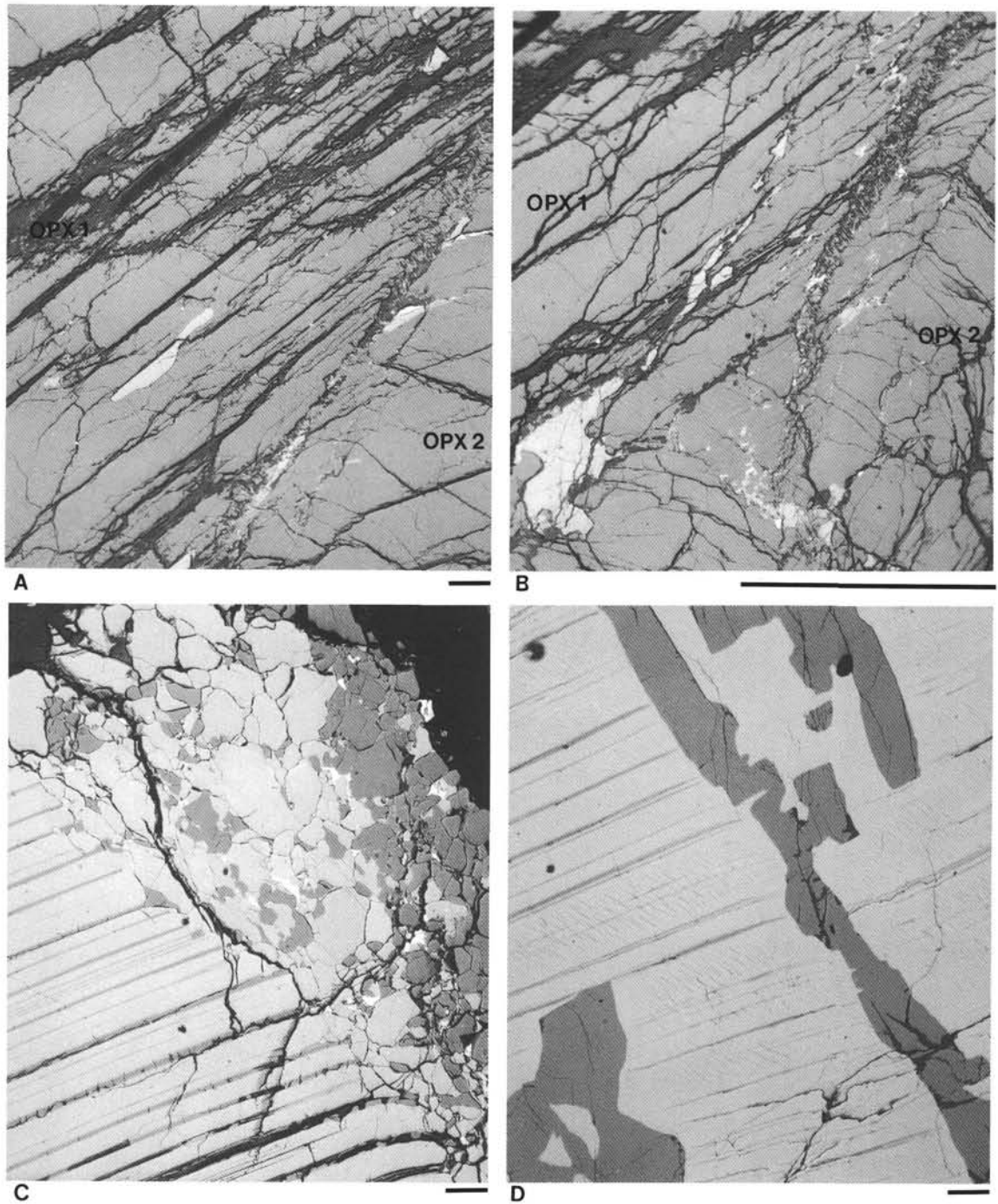


Figure 2. Back-scattered electron images showing the nature of pyroxene exsolution in the Hole 670A peridotites. Orthopyroxene appears dark and clinopyroxene appears light in the photos. **A.** Contact between two orthopyroxene porphyroclasts (OPX 1 and OPX 2) in 109-670A-6R-1, 54–56 cm, both with exsolved clinopyroxene lamellae and blebs. Scale bar = 100  $\mu\text{m}$ . **B.** Another part of same two orthopyroxene grains with blebs of exsolved clinopyroxene. Scale bar = 1000  $\mu\text{m}$ . **C.** Clinopyroxene porphyroclast in 109-670A-6R-1, 54–56 cm. Orthopyroxene lamellae are present in the porphyroclast on the left, and abundant granular orthopyroxene is seen on the right. Granular orthopyroxene is thought to have exsolved from clinopyroxene host. A few small, bright patches of spinel are present. Scale bar = 100  $\mu\text{m}$ . **D.** Exsolved(?) orthopyroxene in a clinopyroxene host in 109-670A-9R-1, 94–97 cm. Scale bar = 100  $\mu\text{m}$ .

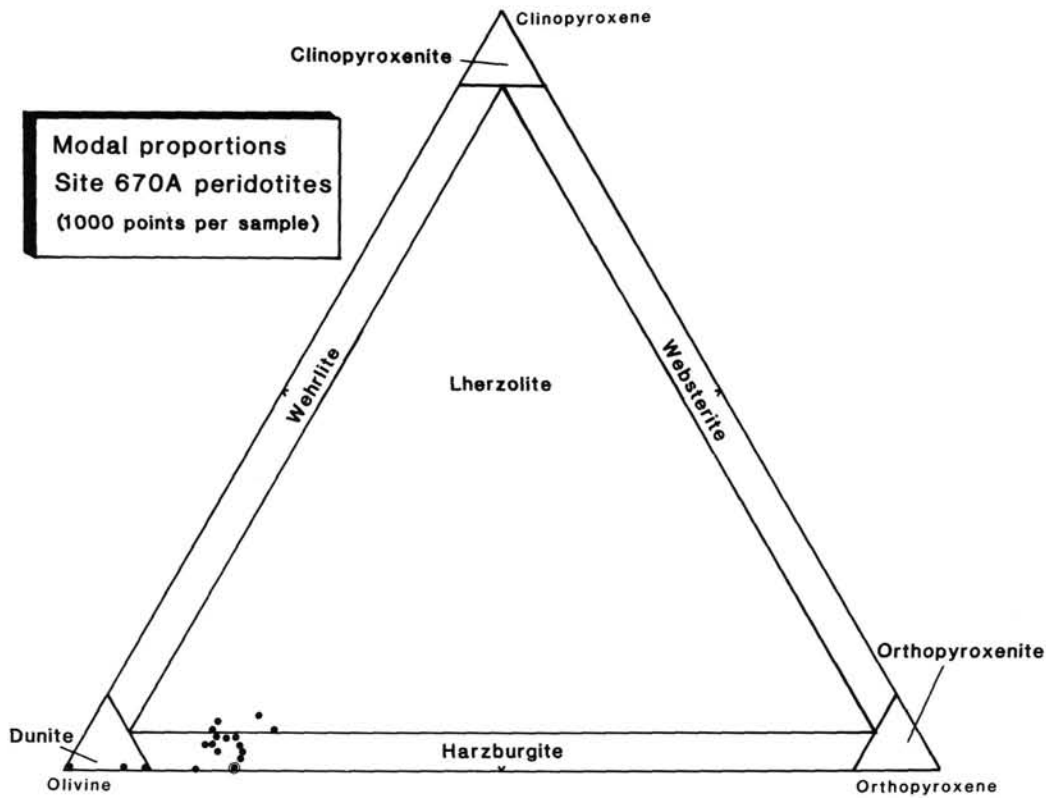


Figure 3. Reconstructed modal proportions for the Hole 670A peridotites. The circled data point is for harzburgite 109-670A-2M-1, 20–23 cm. The boundary between harzburgite and lherzolite occurs at 5% orthopyroxene.

Table 5. Average data for Site 670A peridotites.

	Host <sup>1</sup> CPX	Host <sup>1</sup> OPX	Exsolved <sup>2</sup> CPX	Exsolved <sup>2</sup> OPX	OL	SPIN	Calculated compositions		Measured average whole rock <sup>3</sup>
							CPX- bearing whole rock	2M-1, 20–23 cm whole rock	
Modal proportions	3.40	16.02	0.67	0.29	78.62	1.03			
<sup>4</sup> Density (g/cm <sup>3</sup> )	3.302	3.303	3.300	3.307	3.333	4.000			
SiO <sub>2</sub> (wt%)	50.96	54.65	51.37	54.32	40.56	0.07	42.85	42.90	43.72
TiO <sub>2</sub>	0.13	0.04	0.13	0.03		0.07	0.01	0.01	0.01
Al <sub>2</sub> O <sub>3</sub>	5.13	4.21	4.88	4.70		45.77	1.46	1.09	1.34
Cr <sub>2</sub> O <sub>3</sub>	1.22	0.82	1.12	0.89		22.35	0.46	0.57	0.29
FeO	3.03	5.99	2.85	6.44	9.28	13.57	8.57	8.31	8.05
MnO	0.11	0.16	0.11	0.16	0.14	0.16	0.14	0.12	0.13
MgO	16.93	31.84	16.93	32.00	49.48	18.04	45.03	46.18	44.95
CaO	21.77	1.84	22.38	1.04	0.05		1.22	0.55	0.82
NiO					0.31	0.23	0.25	0.25	0.27
Na <sub>2</sub> O	0.19	0.03	0.21	0.02			0.01	0.02	0.01
Total	99.66	99.59	99.97	99.60	99.85	100.25	100.00	100.00	100.00

<sup>1</sup> Modes of host pyroxenes adjusted for concentrations of exsolved pyroxene.

<sup>2</sup> Modes of exsolved pyroxenes determined by point counting enlarged back-scattered electron photo composites of pyroxene grains.

<sup>3</sup> Measured average whole rock normalized to 100% (L. Autio, unpublished data).

<sup>4</sup> Densities: CPX, Winchell (1961); OPX, Winchell and Leake (1965); OL, Bloss (1952); SPINEL, Deer et al. (1966).

the triangular region at the bottom of the figure contoured for percent melt. This graphical analysis indicates that mixtures of ~13%–14% melt with the Hole 670A calculated average provides the best fit to the Tinaquillo lherzolite composition. Approximately 18%–19% melt added to the Hole 670A average provides the best fit to pyrolite.

The 8-, 10-, and 15-kbar equilibria for mantle melting are plotted as points in Figure 11. However, melting experiments on natural peridotites indicate the liquid compositions in equilibrium with olivine, clinopyroxene, orthopyroxene, and spinel are not isobarically invariant (e.g., Fujii and Scarfe, 1985). The equilibrium liquid compositions change with in-

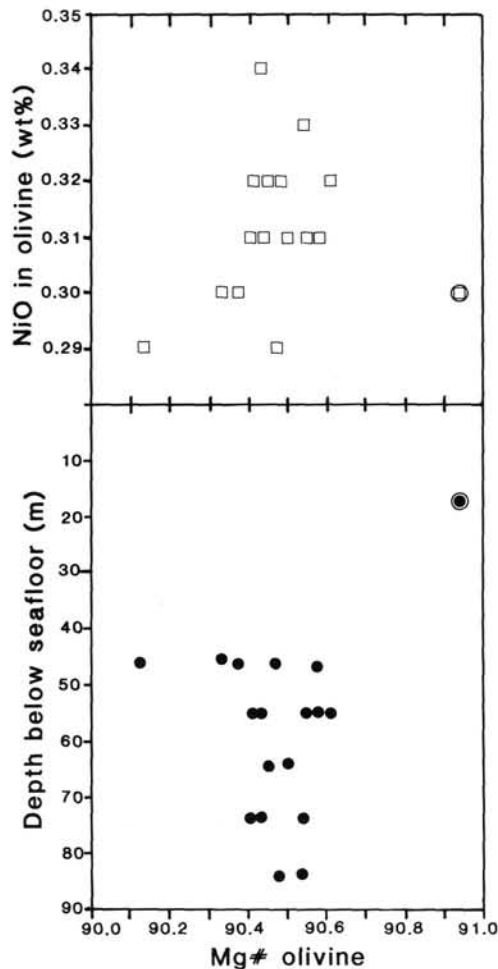


Figure 4. Top. Mg# ( $(100 \times \text{Mg})/(\text{Mg} + \text{Fe})$ ) in olivine vs. NiO in olivine. Bottom. Mg# in olivine vs. depth below the seafloor. No cryptic variation is observed. The circled data point is for harzburgite 109-670A-2M-1, 20–23 cm.

creasing temperature at a given pressure, so the diagram cannot be used as a geobarometer. However, the diagram is still useful for estimating melting percentages, because the 8–15-kbar equilibrium liquid compositions change in the same direction and by similar amounts for a given temperature change (e.g., Thompson, 1987; Fig. 6B).

2. Equilibrium melting percentages can also be estimated using least squares calculations (Bryan, 1986). Table 6 lists compositions for the Hole 670A calculated average, the Tinaquillo lherzolite, and three liquids in equilibrium with olivine, orthopyroxene, clinopyroxene, and spinel at 10 kbar. These particular liquid compositions were chosen because the temperatures at which they are in equilibrium with peridotite range from 1290° to 1300°C, similar to equilibration temperatures estimated by the Lindsley-Anderson geothermometer for reintegrated pyroxene compositions (Fig. 9). Calculations indicate that mixtures of 15%–17% liquid with 83%–85% Hole 670A average provide the best fit to the Tinaquillo lherzolite (Table 6).

The calculation was repeated substituting the calculated whole rock composition of harzburgite 109-670A-2M-1, 20–23 cm, for the Hole 670A average. A mixture of 18%–20% liquid with 80%–82% 109-670A-2M-1, 20–23 cm, provides the best fit to the Tinaquillo lherzolite. This somewhat larger percentage of melting calculated for 109-670A-2M-1, 20–23 cm,

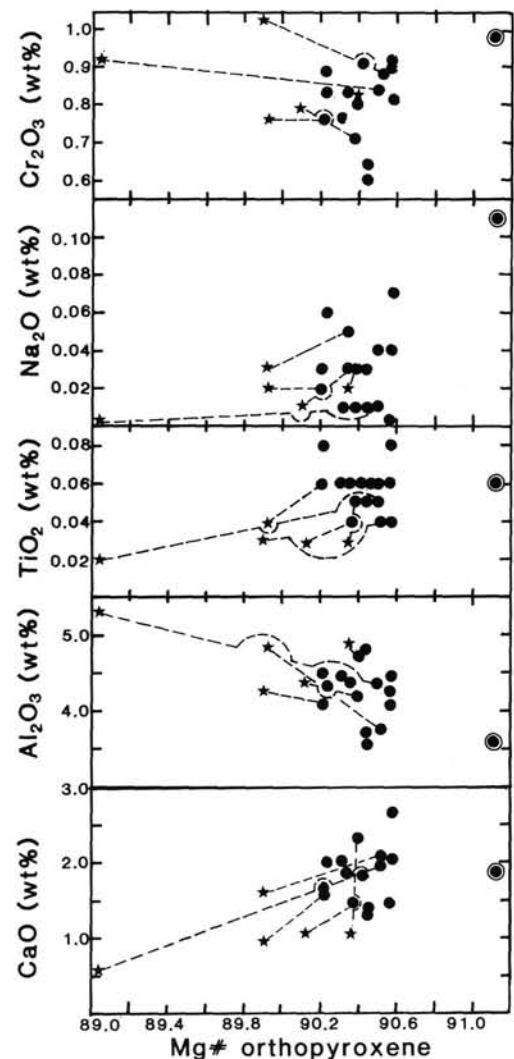


Figure 5. Orthopyroxene mineral chemistry. Tie lines connect orthopyroxene porphyroclasts (●) and orthopyroxene exsolved from clinopyroxene hosts (\*) in the same samples. Compared to orthopyroxene porphyroclasts, exsolved orthopyroxene has lower CaO, higher  $\text{Al}_2\text{O}_3$ , lower  $\text{TiO}_2$ , lower  $\text{Na}_2\text{O}$ , and higher  $\text{Cr}_2\text{O}_3$ . The circled data point is for harzburgite 109-670A-2M-1, 20–23 cm. Except for anomalously high  $\text{Na}_2\text{O}$ , orthopyroxene in this sample is more refractory than in other samples.

compared to the other samples is consistent with its more refractory mineralogical and chemical characteristics.

3. Figure 12 shows concentrations of NiO in olivine vs.  $\text{TiO}_2$  and  $\text{Cr}_2\text{O}_3$  in pyroxene, with calculated curves describing the variation of these oxide concentrations during batch equilibrium melting (Hanson, 1978, equation 10). Parameters used in the modeling are listed in Table 7. The percent melting indicated by average olivine NiO and pyroxene  $\text{TiO}_2$  concentrations is ~14% for clinopyroxene, and 11% for orthopyroxene, whereas  $\text{Cr}_2\text{O}_3$  data for both pyroxenes indicate ~16%–17% melting.

In summary, three methods of estimating the extent of melting suggest that 11%–17% melting of a partially depleted spinel lherzolite like the Tinaquillo lherzolite could produce the Hole 670A average peridotite. A more refined estimate supported by the modeling is 14%–16% melting. The percent melting for harzburgite 109-670A-2M-1, 20–23 cm, may be higher by a small amount (~2%–3%) than for the other samples. This is significant because it suggests that percent-

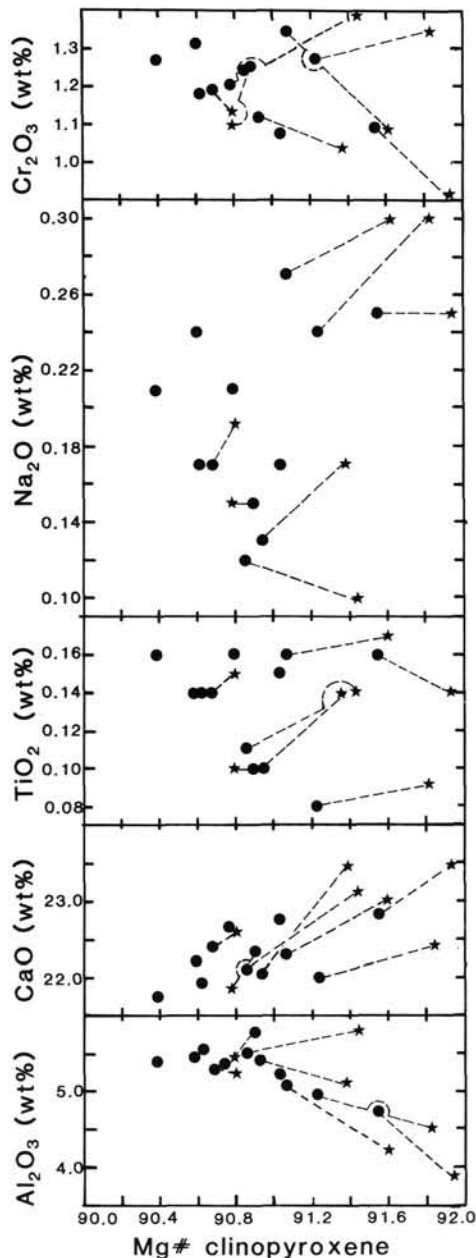


Figure 6. Clinopyroxene mineral chemistry. Tie lines connect clinopyroxene porphyroclasts (●) and exsolved clinopyroxene (★) in orthopyroxene hosts in the same samples. Compared to clinopyroxene porphyroclasts, exsolved clinopyroxene generally has lower Al<sub>2</sub>O<sub>3</sub>, higher CaO, higher TiO<sub>2</sub>, higher Na<sub>2</sub>O, and lower Cr<sub>2</sub>O<sub>3</sub>.

ages of melting (or the efficiency of melt extraction) in upper mantle peridotites may vary over distances of 30 m (i.e., the separation between 109-670A-2M-1, 20–23 cm, and the rest of the samples, assuming no large-offset faulting). Similar decimeter-scale variation in mineralogy and chemistry is observed in the residual mantle portions of some ophiolites, where patchy dunites are gradational into clinopyroxene-free and clinopyroxene-bearing harzburgites (Dick, 1977; Girardeau and Mercier, 1988).

### DISCUSSION

A greater extent of melting in a normal ridge environment compared to a fracture zone setting is predicted by Bender et

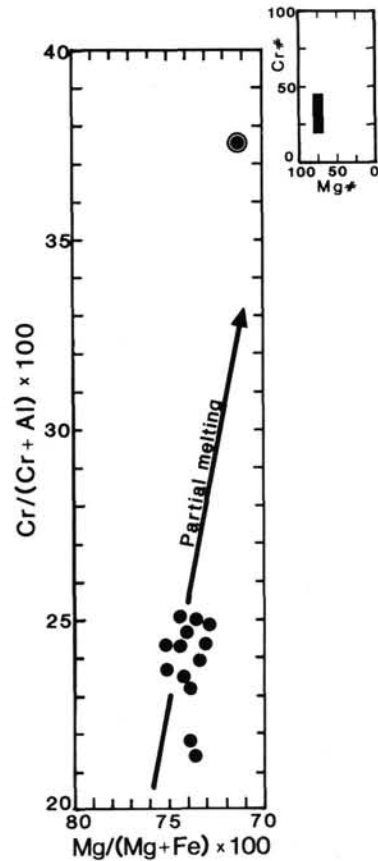


Figure 7. Spinel mineral chemistry. The circled data point is for harzburgite 109-670A-2M-1, 20–23 cm. The arrow shows how spinel mineral chemistry changes during partial melting of peridotite (higher Cr#, lower Mg#; after Dick and Bullen, 1984, Fig. 6a).

al. (1984) to account for the systematic correlation of basalt chemistry with distance from transform faults (transform fault effect). The transform fault effect has been documented for the KFZ by Langmuir and Bender (1984), who show that basalts collected within the fracture zone are enriched in incompatible elements (e.g., TiO<sub>2</sub>) compared to basalts collected >15 km away from the fracture zone along the Mid-Atlantic Ridge. In order to compare the extents of melting of peridotites from the KFZ and the adjacent ridge, parameters that are sensitive to the extent of partial melting are compiled in Table 8 for the Hole 670A samples and for peridotites collected within the KFZ. The compiled data do not consistently indicate a greater extent of melting for the Hole 670A samples, which are more distant from the transform and thus should be more refractory. Considering only the mineral chemistry data, which perhaps are more reliable than the modal data, the majority of the melting parameters suggest that the Hole 670A samples represent *less* melting than the KFZ samples.

One explanation for this result is that the zero-offset transform (ZOT) where the Hole 670A samples were collected does not represent a "normal" ridge-like environment. Upper mantle peridotites that upwell in the ZOT may undergo low degrees of partial melting because they do not supply large amounts of basalt to a constructional spreading ridge. The amount of partial melt that *is* derived from peridotites in the ZOT may be similar to or even less than that required to form the comparatively thin crust found in portions of the KFZ (Karson and Dick, 1983). If this is the case, there is no reason

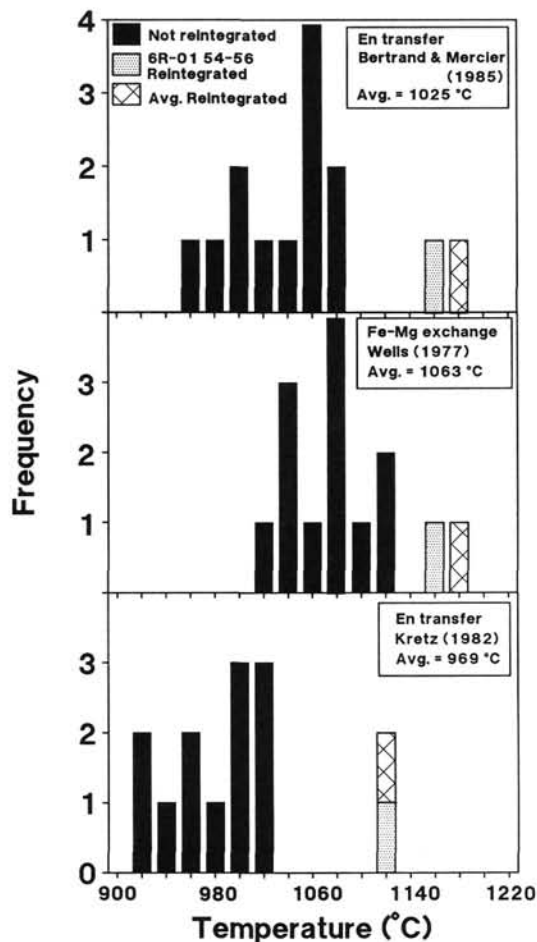


Figure 8. Histograms of two-pyroxene equilibration temperatures calculated by three methods. Host porphyroclastic pyroxene compositions were used to calculate all temperatures, except for two temperatures estimated from reintegrated pyroxene compositions. The pressure term in the Bertrand and Mercier (1985) geothermometer was set to 10 kbar. Temperatures shown here are believed to represent subsolidus reequilibration.

to expect significant differences in the degree of melting of peridotites at Hole 670A compared to the KFZ. Other explanations are possible for the apparent lack of more extensively melted peridotites at Hole 670A compared to the KFZ. One is that the variations in melting percentages are so small as to be undetectable with the methods used in this study. Bender et al. (1984) suggested that differences in melting percentages sufficient to account for the transform fault effect would generate a difference in residual olivine compositions of just  $Fo_{0.5}$ . A further complicating factor arises from the apparent difference in the extent of melting of harzburgite 109-670A-2M-1, 20–23 cm, compared to the rest of the Hole 670A samples. If such local variations in melting are significant, they might mask larger scale patterns of melting. A final explanation for the data is that the transform fault effect may arise from variations in magma chamber processes, rather than from variations in the extent of partial melting of the mantle (Karson and Elthon, 1987).

### CONCLUSIONS

Harzburgites and dunites representing residues of mantle melting are exposed in a 10-km-wide zero-offset transform zone ~45 km south of the KFZ. The chemistry and mineral-

ogy of these samples suggest they formed from 14%–16% partial melting of a source similar to the Tinaquillo spinel lherzolite. The temperature of magmatic equilibration is estimated at 1300°C from reintegrated pyroxene compositions and by comparison with high pressure melting experiments. Comparison of the Hole 670A samples with peridotites from the KFZ provides no strong evidence for differences in the percent melting of upper mantle in the two regions. The thermal environments of the KFZ and the zero-offset transform where the Hole 670A peridotites were collected may be sufficiently similar as to cause no detectable differences in the percent melting of upwelling peridotites.

### ACKNOWLEDGMENTS

This manuscript was written while SCK was a post-doctoral researcher at the University of Wisconsin, Madison. SCK thanks John Valley for support during this period, and S. W. Bailey for access to his x-ray diffraction laboratory.

### REFERENCES

- Albee, A. L., and Ray L., 1970. Correction factors for electron probe microanalysis of silicates, oxides, carbonates, phosphates and sulfates. *Anal. Chem.*, 42:1408–1414.
- Anderson, D. J., and Lindsley, D. H., 1984. Application of a two-pyroxene thermometer: correlation of apparent temperature with  $Al_2O_3$  in augite. *Lunar Planet. Sci.* 15:7–8.
- Barth, T. F. W., 1962. *Theoretical Petrology*: New York (Wiley).
- Bence, A. E., and Albee, A. L., 1968. Empirical correction factors for the electron microanalysis of silicates and oxides. *J. Geol.*, 76:382–403.
- Bender, J. F., Langmuir, C. H., and Hanson, G. H., 1984. Petrogenesis of basalt glasses from the Tamayo region, East Pacific Rise. *J. Petrol.*, 25:215–234.
- Bertrand, P., and Mercier, J-C. C., 1986. The mutual solubility of coexisting ortho- and clinopyroxene: toward an absolute geothermometer for the natural system? *Earth Planet. Sci. Lett.*, 76: 109–122.
- Bloss, F. D., 1952. Relationship between density and composition in mol. per cent. for some solid solution series. *Am. Mineral.*, 37:966–981.
- Bonatti, E., Lawrence, J. R., and Morandi, N., 1984. Serpentinization of oceanic peridotites: temperature dependence of mineralogy and boron content. *Earth. Planet. Sci. Lett.*, 70:88–94.
- Boudier, F., 1979. Microstructural study of three peridotite samples drilled at the western margin of the Mid-Atlantic Ridge. In Melson, W. G., Rabinowitz, P. D., et al., *Init. Repts. DSDP*, 45: Washington (U.S. Govt. Printing Office), 603–608.
- Bryan, W. B., 1986. Linked evolutionary data arrays: a logical structure for petrologic modeling of multisource, multiprocess magmatic systems. *J. Geophys. Res.*, 91:5891–5900.
- Campbell, A. C., Palmer, M. R., Klinkhammer, G. P., et al., 1988. Chemistry of hot springs on the Mid-Atlantic Ridge. *Nature*, 335:514–519.
- Casey, J. F., Dewey, J. F., Fox, P. J., Karson, J. A., and Rosenkrantz, J., 1981. Heterogeneous nature of oceanic crust and upper mantle: a perspective from the Bay of Islands ophiolite. In Emiliani, C. (Ed.), *The Sea*, 7: New York (Wiley), 305–338.
- Clayton, R. N., and Mayeda, T. K., 1963. The use of bromine pentafluoride in the extraction of oxygen from oxide and silicates for analysis. *Geochim. Cosmochim. Acta*, 32:43–52.
- Conrad, W. K., and Kay, R. W., 1984. Ultramafic and mafic inclusions from Adak Island: Crystallization history, and implications for the nature of primary magmas and crustal evolution in the Aleutian Arc. *J. Petrol.*, 25:88–125.
- Cox, K. G., Bell, J. D., and Pankhurst, R. J., 1979. *The Interpretation of Igneous Rocks*: London (Allen and Unwin).
- Craig, H., 1961. Standard for reporting concentrations of deuterium and oxygen-18 in natural waters. *Science*, 154:1544–1548.
- Deer, W. A., Howie, R. A., Zussman, J., 1966. *An Introduction to the Rock-Forming Minerals*: London (Longman).
- Dick, H.J.B., 1977. Partial melting in the Josephine Peridotite I, the effect on mineral composition and its consequence for geobarometry and geothermometry. *Am. J. Sci.*, 277:801–832.

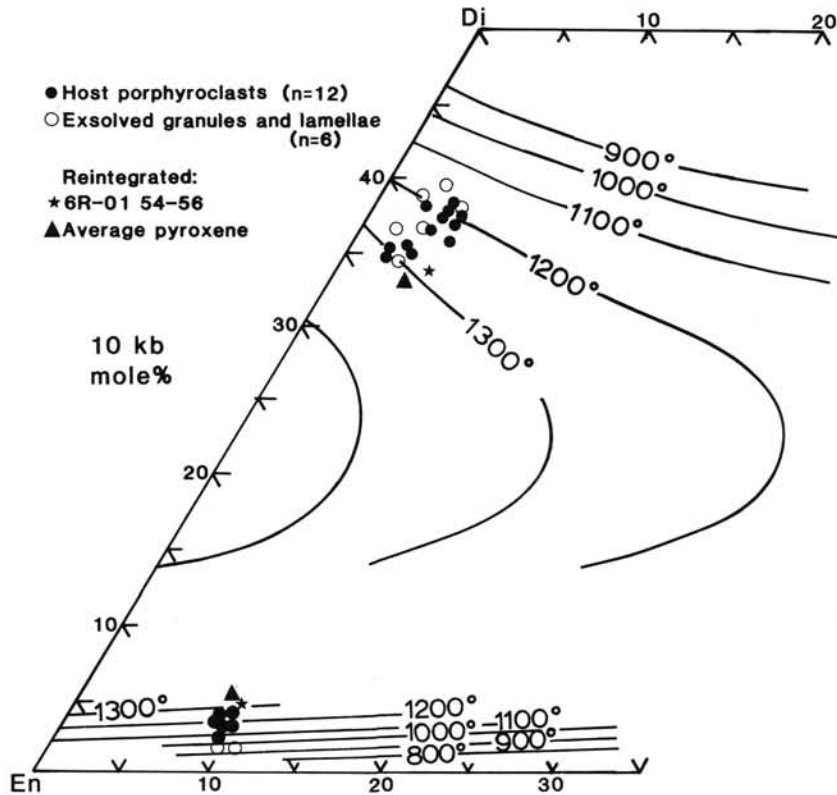


Figure 9. Part of the 10-kbar pyroxene geothermometer of Lindsley and Anderson (1983). Reintegrated pyroxene compositions indicate equilibration temperatures of  $\sim 1300^{\circ}\text{C}$ , which is considered a reasonable estimate of the temperature of magmatic equilibration. Overlap of data points prevents all of the orthopyroxene data from being visible.

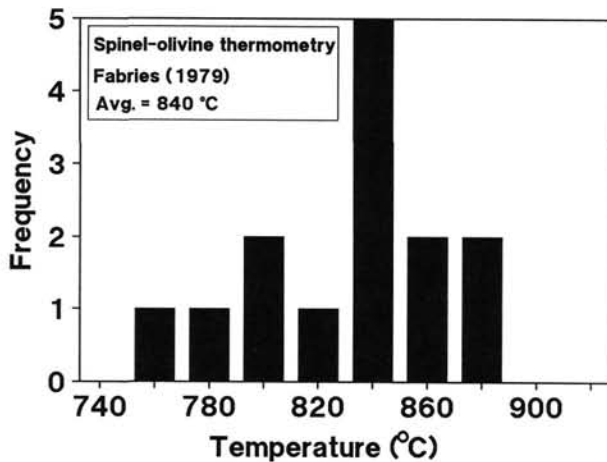


Figure 10. Histogram of temperatures calculated from olivine-spinel Mg-Fe exchange equilibrium. Temperatures represent subsolidus reequilibration.

- Dick, H.J.B., and Bullen, T., 1984. Chromian spinel as a petrogenetic indicator in abyssal and alpine-type peridotites and associated lavas. *Contrib. Mineral. Petrol.*, 86:54-76.
- Dick, H.J.B., and Fisher, R. L., 1983. Mineralogic studies of the residues of mantle melting: abyssal and alpine-type peridotites. In Kornprobst, J. (Ed.), *Proceedings of the Third International Kimberlite Conference*, Amsterdam (Elsevier), 295-308.
- Dick, H.J.B., Fisher, R. L., and Bryan, W. B., 1984. Mineralogic variability of the uppermost mantle along mid-ocean ridges. *Earth Planet. Sci. Lett.*, 69:88-106.

- Elthon, D., 1987. Partitioning of Ni between olivine and high-MgO basaltic liquids. *Proc. Lunar Planet. Sci. Conf.*, 18:258-259.
- Elthon, D. E., Casey, J. F., and Komor, S. C., 1982. Mineral chemistry of ultramafic cumulates from the North Arm Mountain massif of the Bay of Islands ophiolite: evidence of high-pressure crystal fractionation of oceanic basalts. *J. Geophys. Res.*, 87:8717-8734.
- Evans, B. W., Johannes, W., Oterdsom, H., and Trommsdorff, V., 1976. Stability of chrysotile and antigorite in the serpentinite multsystem. *Schweiz. Mineral. Petrogr. Mitt.*, 56:79-93.
- Fabries, J., 1979. Spinel-olivine geothermometry in peridotites from ultramafic complexes. *Contrib. Mineral. Petrol.*, 69:329-336.
- Frey, F. A., 1983. Rare earth abundances in upper mantle rocks. In Henderson, P. (Ed.), *Rare Earth Element Geochemistry*: Amsterdam (Elsevier), 153-203.
- Fujii, T., and Bougault, H., 1983. Melting relations of a magnesian abyssal tholeiite and the origin of MORBs. *Earth Planet. Sci. Lett.*, 62:283-295.
- Fujii, T., and Scarfe, C. M., 1985. Compositions of liquids coexisting with spinel lherzolite at 10 kbar and the genesis of MORBs. *Contrib. Mineral. Petrol.*, 90:18-28.
- George, R. P., 1978. Structural petrology of the Olympus ultramafic complex in the Troodos ophiolite, Cyprus. *Bull. Geol. Soc. Am.*, 89:845-865.
- Girardeau, J., and Mercier, J.-C. C., 1988. Petrology and texture of the ultramafic rocks of the Xigaze ophiolite (Tibet): constraints for mantle structure beneath slow-spreading ridges. *Tectonophysics*, 147:33-58.
- Grove, T. L., and Bryan, W. B., 1983. Fractionation of pyroxenophytic MORB at low pressure: An experimental study. *Contrib. Mineral. Petrol.*, 84:293-309.
- Hanson, G. H., 1978. The application of trace elements to the petrogenesis of igneous rocks of granitic composition. *Earth Planet. Sci. Lett.*, 38:26-43.
- Harper, G. D., Bowman, J. R., and Kuhns, R., 1988. A field, chemical and stable isotope study of seafloor metamorphism of the

## Abyssal peridotites

Site 670A

● Calculated

■ Measured

Global averages

□ Dick &amp; Fisher, 1983

◆ less refractory } Michael &amp;

○ more refractory } Bonatti, 1985

## Upper mantle analogs

☆ Pyrolite (Ringwood, 1975)

★ Tinaquillo lherzolite (Jaques &amp; Green, 1980)

## Equilibrium liquids

LIQ+OL+OPX+CPX+SPIN,

10 kb, 1290–1300°C

■ SM-4 Run #242 (Fujii &amp; Scarfe, 1985)

▲ ARP 74 Run #T3 (Fujii &amp; Bougault, 1983)

⊠ Tinaquillo melt Run #T-128 (Jaques &amp; Green, 1980)

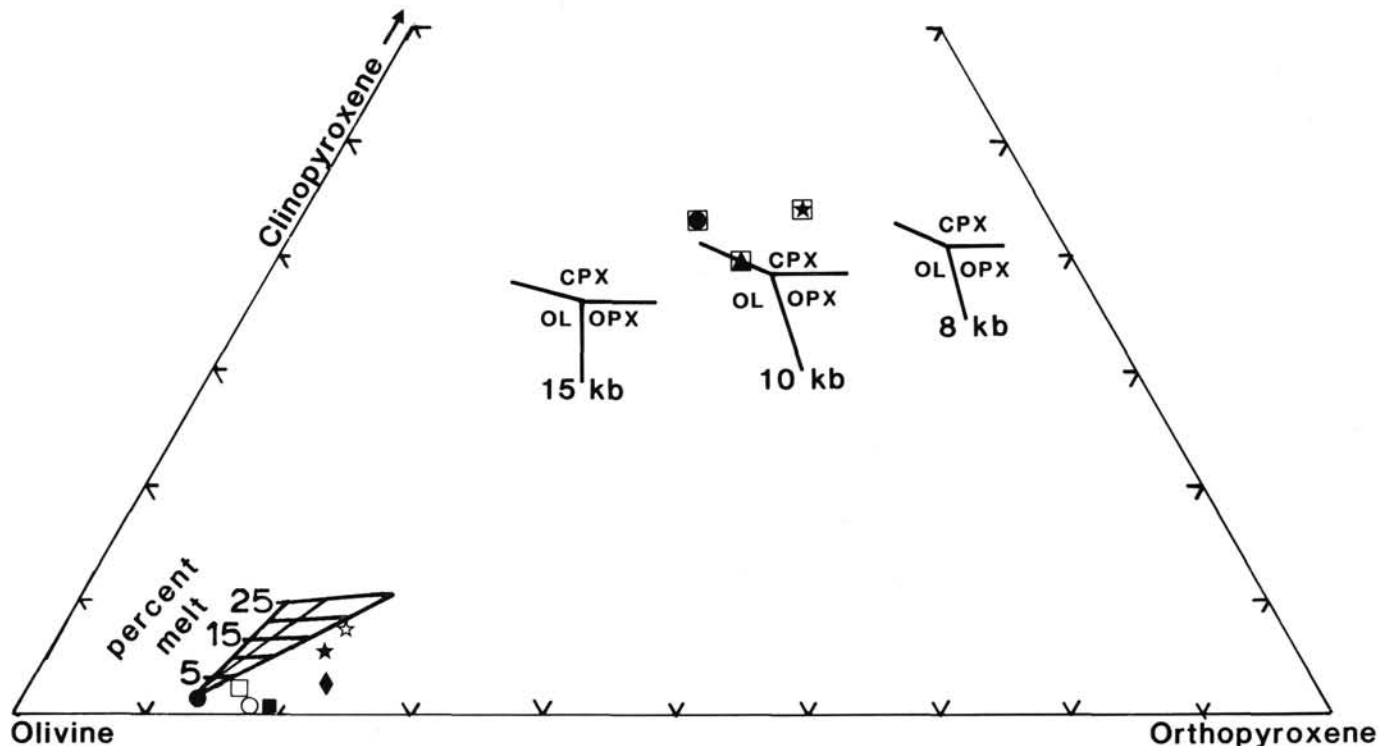


Figure 11. Normative olivine-clinopyroxene-orthopyroxene (Ol-Di-Hy in cation norm of Barth, 1962). High pressure phase boundaries are from Takahashi and Kushiro (8 kbar) and Stolper (10 and 15 kbar). The triangular region at the lower left shows how the composition of the calculated Hole 670A whole rock composition (●) changes with addition of up to 25% equilibrium liquid. The best fit to the Tinaquillo lherzolite (★), an appropriate MORB-source mantle) results from addition of ~13%–14% melt with the Hole 670A average whole rock. Shown for comparison are the measured Hole 670A average (L. Autio, unpubl. data), and calculated average abyssal peridotite compositions (mostly from fracture zones) from Dick and Fisher (1983) and Michael and Bonatti (1985).

- Josephine ophiolite, California-Oregon. *J. Geophys. Res.*, 93: 4625–4656.
- Hebert, R., Bideau, D., and Hekinian, R., 1983. Ultramafic and mafic rocks from the Garret Transform Fault near 13°30' on the East Pacific Rise: igneous petrology. *Earth Planet. Sci. Lett.*, 65:107–125.
- Henderson, P., 1982. *Inorganic Geochemistry*: Oxford (Pergamon).
- Hodges, F. H., and Papike, J. J., 1976. DSDP Site 334: Magmatic cumulates from oceanic layer 3. *J. Geophys. Res.*, 81:4135–4151.
- Irvine, T. N., and Smith, C. H., 1967. The ultramafic rocks of the Muskox intrusion. In Wyllie, P. J. (Ed.), *Ultramafic and Related Rocks*: New York (Wiley), 38–49.
- Janecky, D. R., and Seyfried, W. E., 1986. Hydrothermal serpentinization of peridotite within the oceanic crust: Experimental investigations of mineralogy and major element chemistry. *Geochim. Cosmochim. Acta*, 50:1357–1378.
- Jaques, A. L., and Green, D. H., 1980. Anhydrous melting of peridotite at 0–15 kb pressure and the genesis of tholeiitic basalts. *Contrib. Mineral. Petrol.*, 73:287–310.
- Karson, J. A., and Dick, H. J. B., 1983. Tectonics of ridge-transform intersections at the Kane Fracture Zone. *Mar. Geophys. Res.*, 6:51–99.
- Karson, J. A., and Elthon, D. E., 1987. Evidence for variations in magma production along oceanic spreading centers: a critical appraisal. *Geology*, 15:127–131.
- Karson, J. A., Thompson, G., Humphris, S. E., et al., 1987. Along-axis variations in seafloor spreading in the MARK area. *Nature*, 328:681–685.
- Komor, S. C., Elthon, D. E., and Casey, J. F., 1985. Serpentinization of cumulate ultramafic rocks from the North Arm Mountain massif of the Bay of Islands ophiolite. *Geochim. Cosmochim. Acta*, 49:2331–2338.
- Kretz, R., 1982. Transfer and exchange equilibria in a portion of the pyroxene quadrilateral as deduced from natural and experimental data. *Geochim. Cosmochim. Acta*, 46:411–421.
- Lange, D. E., and Recca, S. I., 1987. MINQUANT II: A mineral code soft key program for Sandia task8. In Geiss, R. H. (Ed.), *Microbeam Analysis—1987*: San Francisco (San Francisco Press), 348.
- Langmuir, C. H., and Bender, J. F., 1984. The geochemistry of oceanic basalts in the vicinity of transform faults: Observations and implications. *Earth Planet. Sci. Lett.*, 69:107–127.

Table 6. Least Squares Modeling of Melting—Whole Rock Compositions

Wt% oxide	Model MORB-source mantle	Model Equilibrium melts of MORB-source mantle			Model Residues of mantle-melting	
	Tinaquillo lherzolite(1)	Tinaquillo melt(1)	SM-4(2)	ARP 74(3)	Site 670A calculated whole rocks	
					Average(4)	2M-01 20-23
SiO <sub>2</sub>	44.95	49.00	49.30	50.00	42.85	42.90
TiO <sub>2</sub>	0.08	0.30	0.63	0.85	0.01	0.01
Al <sub>2</sub> O <sub>3</sub>	3.22	14.80	15.40	16.00	1.46	1.09
FeO	7.66	8.14	7.23	8.00	8.57	8.37
MnO	0.14	0.20	0.11	0.14	0.14	0.12
MgO	40.03	13.70	12.20	9.97	45.03	46.18
CaO	2.99	12.60	12.20	11.80	1.22	0.55
Na <sub>2</sub> O	0.26	1.10	1.84	2.20	0.01	0.02
Total	99.20	99.84	98.91	98.96	100.00	100.00
Best-fit proportions						
Melt%	17.0	16.5	15.6	(Residue is 670A average)		
Residue%	83.0	83.5	84.4			
Σr <sup>2</sup>	1.5	1.2	1.4			
FeO <sup>-</sup>	+1.0	+0.8	+1.0	Largest three (calculated-observed) differences		
Al <sub>2</sub> O <sub>3</sub> <sup>-</sup>	+0.6	+0.6	+0.6			
SiO <sub>2</sub> <sup>-</sup>	-0.4	-0.4	-0.3			
Melt%	19.8	19.1	18.1	(Residue is 2M-01 20-23)		
Residue%	80.2	80.9	81.9			
Σr <sup>2</sup>	1.1	0.9	1.1			
FeO	+0.7	+0.7	+0.7	Largest three (calculated-observed) differences		
Al <sub>2</sub> O <sub>3</sub>	+0.6	+0.5	+0.6			
SiO <sub>2</sub>	-0.4	-0.3	—			
CaO	—	—	-0.4			

<sup>1</sup> Jaques and Green (1980).

<sup>2</sup> Fujii and Scarfe (1985).

<sup>3</sup> Fujii and Bougault (1983).

<sup>4</sup> Average of CPX-bearing samples.

<sup>5</sup> Elemental names used as abbreviations for oxides.

- Lindsley, D. H., and Anderson, D. J., 1983. A two-pyroxene thermometer. *J. Geophys. Res.*, 88:A887-A906.
- Maurel, C., and Maurel, P., 1982. Experimental investigation of chromium solubility in basic silicate melts and of chromium distribution between liquid and coexisting minerals: conditions of existence of chromian spinel. *Bull. Mineral.*, 105:640-647.
- Michael, P. J., and Bonatti, E., 1985. Peridotite compositions from the North Atlantic: regional and tectonic variations and implications for partial melting. *Earth. Planet. Sci. Lett.*, 73:91-104.
- Mysen, B. O., and Kushiro, I., 1977. Compositional variations of coexisting phases with degree of melting of peridotite in the upper mantle. *Am. Mineral.*, 62:843-865.
- Nicolas, A., and Violette, J. F., 1982. Mantle flow at oceanic spreading centers: models derived from ophiolites. *Tectonophysics*, 81:319-339.
- Pearce, J. A., and Norry, M. J., 1979. Petrogenetic implications of Ti, Zr, Y, and Nb variation in volcanic rocks. *Contrib. Mineral. Petrol.*, 69:33-47.
- Phillips, W. R., and Griffen, D. T., 1981. *Optical Mineralogy, The Nonopaque Minerals*: San Francisco (W.H. Freeman).
- Purdy, G. M., Rabinowitz, P. D., and Schouten, H., 1978. The Mid-Atlantic Ridge at 23°N: Bathymetry and Magnetics. In Melson, W. G., Rabinowitz, P. D., et al., *Init. Repts. DSDP*, 45: Washington (U.S. Govt. Printing Office), 119-128.
- Recca, S. I., Lange, D. E., and Grove, T. L., 1987. MINQUANT I: A quantitative analysis schedule for Tracor Northern tasks. In Geiss, R. H. (Ed.), *Microbeam Analysis—1987*: San Francisco (San Francisco Press), 346-347.
- Ringwood, A. E., 1975. *Chemical composition and petrology of the Earth's mantle*. New York (McGraw-Hill).
- Stolper, E., 1980. A phase diagram for mid-ocean ridge basalts: preliminary results and implications for petrogenesis. *Contrib. Mineral. Petrol.*, 74:13-27.
- Stroup, J. B., and Fox, P. J., 1981. Geologic investigations in the Cayman Trough: Evidence for thin crust along the Mid-Cayman Rise. *Geology*, 89:395-420.
- Takahashi, E., and Kushiro, I., 1983. Melting of a dry peridotite at high pressures and basalt magma genesis. *Am. Mineral.*, 68:859-879.
- Thompson, R. N., 1987. Phase-equilibria constraints on the genesis and magmatic evolution of oceanic basalts. *Earth Sci. Rev.*, 24:161-210.
- Van der Plas, L., and Tobi, A. C., 1965. A chart for determining the reliability of point counting results. *Am. J. Sci.*, 263:87-90.
- Wells, P.R.A., 1977. Pyroxene thermometry in simple and complex systems. *Contrib. Mineral. Petrol.*, 62:129-139.
- Wenner, D. B., and Taylor, H. P., 1971. Temperatures of serpentinization of ultramafic rocks based on <sup>18</sup>O/<sup>16</sup>O fractionation between coexisting serpentine and magnetite. *Contrib. Mineral. Petrol.*, 32:165-185.
- Whittaker, E.J.W., and Zussman J., 1956. The characterization of serpentine minerals by x-ray diffraction. *Mineral. Mag.*, 233:107-126.
- Winchell, H., 1961. Regressions of physical properties on the compositions of clinopyroxenes II. Optical properties and specific gravity. *Am. J. Sci.*, 259:259-319.
- Winchell, H., and Leake, B. E., 1965. Regression of refractive indices, density and lattice constants on the composition of orthopyroxenes. *Am. Mineral.*, 50:294.

Date of initial receipt: 28 March 1988

Date of acceptance: 20 April 1989

Ms 106/109B-128

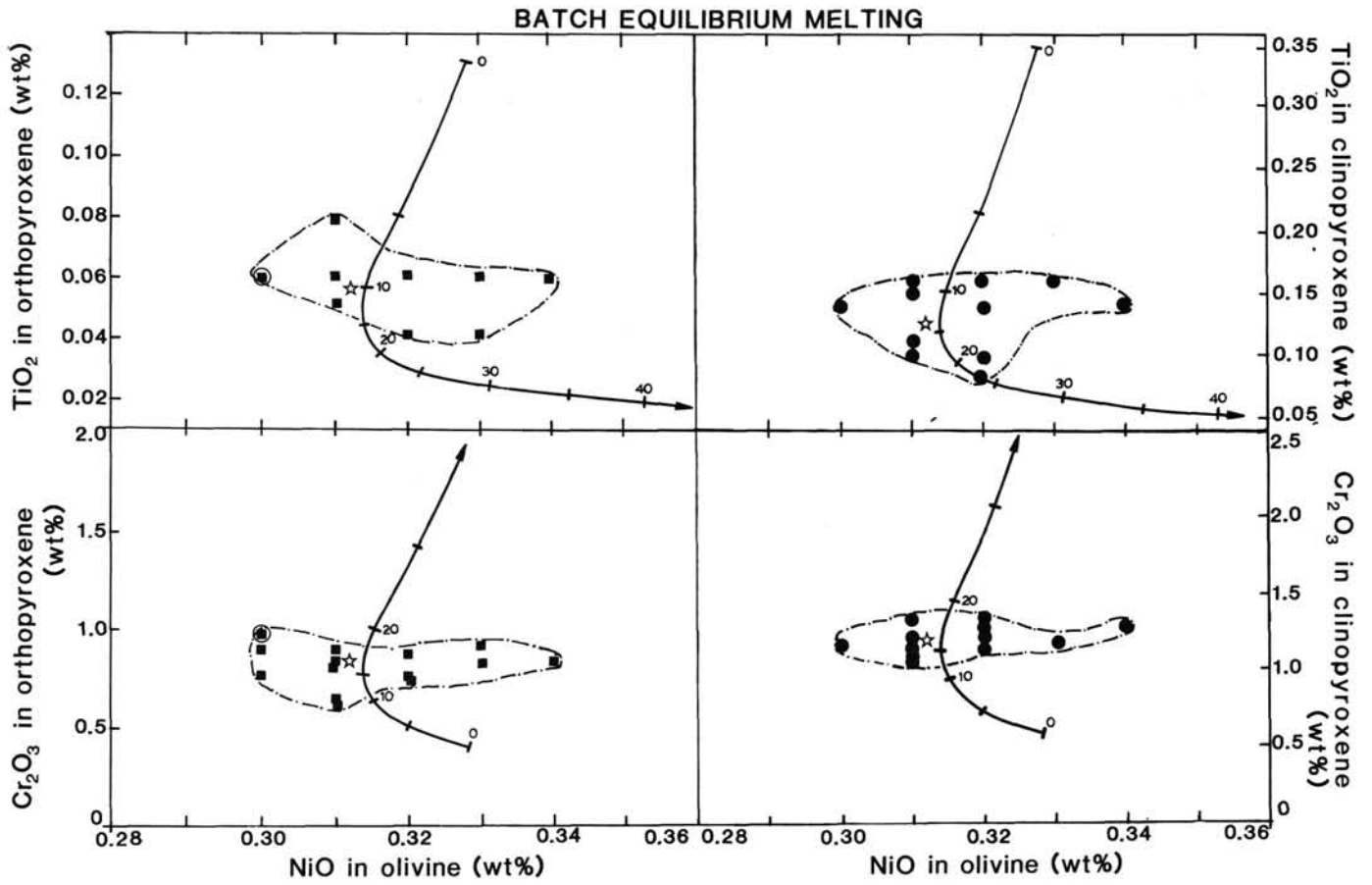


Figure 12. Olivine and pyroxene mineral chemistry variations in the Hole 670A samples with calculated batch equilibrium melting trends. Parameters used to calculate the trends are given in Table 7. The average values for each data set (\*) indicate that ~11%–17% partial melting of the Tinaquillo lherzolite source composition can account for the compositions of the Hole 670A peridotites. Circled data point is 109-670A-2M-1, 20–23 cm.

Table 7. Parameters used in trace element modeling of melting.

Initial composition: NiO - 0.26 wt%.  
 TiO<sub>2</sub> - 0.08 wt%.  
 Cr<sub>2</sub>O<sub>3</sub> - 0.45 wt.

(Tinaquillo lherzolite, Jaques and Green, 1980)

Initial modal proportions: OL - 67% OPX - 23% CPX - 8% SPIN - 2%  
 (Average composition of Lizard lherzolite, Green, 1964).

CPX melts out after 25% melting, OPX melts out after 40% melting.

Distribution Coefficients ( $C_s/C_l$ ) (parenthetical numbers refers to explanatory notes)				
	OL	CPX	OPX	SPIN
NiO	depends on MgO (1)	$0.25 \times D_{NiO-OL}$ (2)	5 (3)	$0.72 \times D_{NiO-OL}$ (4)
Cr <sub>2</sub> O <sub>3</sub>	0.2 (10)	16 (5)	10.7 (6)	420 (7)
TiO <sub>2</sub>	0.02 (8)	0.27 (5)	0.1 (8)	0.14 (9)

<sup>1</sup>  $D_{NiO}^{Olivine} = 122.16 / (wt\% \text{ MgO in liquid}) - 2.27$  (Elthon, 1987). MgO in liquid calculated from regression of wt% MgO in liquid and percent melt from Jaques and Green's (1980) melting experiments on Tinaquillo lherzolite (wt% MgO in liq =  $0.38 \times \% \text{ melt} + 8.30$ ;  $r^2 = 0.98$ ).

<sup>2</sup> Conrad and Kay (1984).

<sup>3</sup> Henderson (1982).

<sup>4</sup> Average Hole 670A NiO in spinel/NiO in olivine (0.72)  $\times D_{NiO-olivine}$ .

<sup>5</sup> Grove and Bryan (1983).

<sup>6</sup> Average Hole 670A Cr<sub>2</sub>O<sub>3</sub> in OPX/Cr<sub>2</sub>O<sub>3</sub> in CPX (0.67)  $\times D_{Cr_2O_3-CPX}$ .

<sup>7</sup> Maurel and Maurel (1982).

<sup>8</sup> Pearce and Norry (1979).

<sup>9</sup> Average Hole 670A TiO<sub>2</sub> in spinel/TiO<sub>2</sub> in CPX (0.52)  $\times D_{TiO_2-CPX}$ .

<sup>10</sup> Cox, Bell, and Pankhurst (1979).

Table 8. Comparison of partial melting parameters for peridotites from Hole 670A and the Kane Fracture Zone (KFZ).

	Inc. or Dec. with <u>melting ?</u>	Site 670A	KFZ		%melting 670A > or < KFZ?	
			(1)	(2)	(1)	(2)
Modal OL	Inc.	78.6	76.5	73.0	>	>
Modal CPX	Dec.	3.3	2.95	0.5	<	<
Mg# OPX	Inc.	90.2	91.4	90.2	<	same
Al <sub>2</sub> O <sub>3</sub> OPX (wt%)	Dec.	4.2	4.0	4.9	<	>
Cr# in spinel	Inc.	24.7	38.0	28.0	<	<

The modal data for Hole 670A is for CPX-bearing samples. The average mode for all samples includes 81.6% OL and 2.4% CPX.

<sup>1</sup> Dick et al. (1984).

<sup>2</sup> Michael and Bonatti (1985).